Northwest Atlantic   Fisheries Organization

SCIENTIFIC COUNCIL MEETING – JUNE 2024

2023 Oceanographic Conditions in the Labrador Sea in the Context of Seasonal, Interannual and Multidecadal Changes

Igor Yashayaev

Fisheries and Oceans Canada – Bedford Institute of Oceanography
P.O. Box 1006, 1 Challenger Drive, Dartmouth, Nova Scotia B2Y 4A2

Abstract

In the Labrador Sea, the coldest and freshest North Atlantic basin south of the Greenland-Scotland Ridge, high winter surface heat losses result in the formation of a cold, fresh and dense water mass water mass, Labrador Sea Water, that sinks to the intermediate and deep layers and spreads across the ocean, contributing to the global ocean overturning circulation, and playing an important role in renewing and ventilating the deep ocean reservoir. This process – convective mixing – undergoes multi-year cycles of intensification (deepening) and relaxation (shoaling), which have been also shown to modulate long-term changes in the atmospheric gas uptake by the sea. The most recent convective cycle started in 2012, following two consecutive years of shallow winter mixing. Convection progressed deepening year by year until 2018, when it became the deepest for the entire 1996-2023 period. However, the highest winter cooling for the 1994-2023 period was in 2015, while the deepest convection occurred three years later. This time lag was due to the preconditioning of the water column by the 2012-2015 winter mixing events, making it susceptible to deep convection in three more years. The progressive deepening of winter convection from 2012 to 2018 (exceeding the depth of 2000 m in 2018) generated the largest, densest and deepest class of Labrador Sea Water since 1995. Convection weakened afterwards, rapidly shoaling by 800 m per year in the winters of 2021 and 2023 relative to 2020 and 2022, respectively. Distinct processes were responsible for these two convective shutdowns. In 2021, a collapse and an eastward shift of the stratospheric polar vortex, and a weakening and a southwestward shift of the Icelandic Low resulted in extremely low surface cooling and convection depth. In 2023, by contrast, convective shutdown was caused by extensive upper layer freshening originated from extreme Arctic sea-ice melt due to Arctic Amplification of Global Warming.

In 2023, the central Labrador Sea experienced a near-normal cumulative surface heat loss, which was much higher than in 2021. The 2023 winter (Dec-Mar) North Atlantic Oscillation, Arctic Oscillation and Stratospheric Polar Vortex indices were also near-normal. However, in 2023, winter convection was 100 m shallower than in 2021, with below-normal winter cooling, and the shallowest since 2010, emphasising the prevailing role of freshening in control of winter convection in 2023.

With respect to temperature anomalies averaged annually over the central Labrador Sea, in the 2002-2023 period that was sufficiently covered with profiling Argo float measurements, the upper 100 m layer was the coldest in 2015 and 2018. Following 2018, this layer attained above-normal annual men temperatures during 2019-2023, becoming the warmest for the 2011-2023 period in

2023. The intermediate, 200-2000 m, layer of the Labrador Sea started to cool immediately after reaching its warmest state for the 1972-2023 period in 2011. This persistent 2012-2018 cooling trend was imposed on the intermediate layer by the progressive deepening of winter convection over the same period. The situation changed in 2019, with the depth of winter convection eventually reducing to 800 m in 2021, and then to less than 700 m in 2023. As a result, the intermediate layer has been warming since 2019. The corresponding annual density decreases contributed to a negative 2018-2023 density trend. Between 2018 and 2023, the annual mean intermediate layer density reduced by more than 0.02 kg/m^3.

The freshening of the upper 100 m layer that occurred after 2017 reversed after reaching its peak in 2022. However, the 300-700 m layer continued to freshen in 2023, even showing the largest annual freshening rate ever recorded. As a result, this layer exhibited a persistent six-year, 2018-2023, freshening trend, attributed to the effect of Arctic freshwater discharge on the Labrador Sea. With respect to the intermediate, 200-2000 m, layer as a whole, the freshening trend also persisted through the same, 2018-2023, period.

The reduction in the depth of winter convection in 2023 led to a decrease in the dissolved oxygen concentration below 600 m.

Sea ice area from Davis Strait to southern Labrador Sea decreased between 2022 and 2023 to near-normal.

Introduction

The Labrador Sea is located between Greenland and the Labrador coast of eastern Canada, with its deep semi-enclosed basin bounded by the West Greenland and the Newfoundland-Labrador shelves. Cold, low-salinity waters of polar origin circle the Labrador Sea in a counterclockwise current system that includes both the northward flowing West Greenland Current (WGC) on the eastern side and the southward flowing Labrador Current (LC) on the western side (Figure 1). Distinctively warmer and saltier patches of water can be found underneath the offshore extensions of the WGC and LC. These are variations of the Atlantic Water originating in the low latitudes of the Atlantic Ocean, and following first the North Atlantic Current and then the Gulf Stream. As the Atlantic Water flows into and around the Labrador Sea, following its eastern, northern, and eventually western boundaries, it mixes with other masses, progressively cooling and freshening.

Spatial distribution and temporal changes in temperature, salinity, density, dissolved oxygen, and other environmental variables in the upper and deep layers of the Labrador Sea respond to a wide range of external and internal oceanic factors. The external factors include exchanges with land (e.g., continental runoff), atmosphere (e.g., radiation, latent and sensible heat, and momentum fluxes), precipitation, evaporation, and exchanges with other substances (such as anthropogenic gases). The internal factors include inflows of warmer and saltier, and colder and fresher waters from the adjacent North Atlantic and Arctic, respectively, and local oceanic processes such as lateral mixing and winter convection. Naturally, the physical, chemical, and biological processes and seawater properties are subjected, both vertically and horizontally, to seasonal, interannual, and decadal variations across the region. In addition, instantaneous conditions and process development depend on the cumulative effect of past heat, salt, and freshwater gains and respective temperature, salinity, and density changes termed as ocean preconditioning (Yashayaev and Loder 2017).

The Atlantic Repeat hydrography 7-West (AR7W in Figure 1, Table in *Appendix*) line running across the Labrador Sea for approximately 900 km from Misery Point, Labrador, to Cape Desolation, Greenland, was annually surveyed by the Bedford Institute of Oceanography (BIO) of Fisheries and Oceans Canada (DFO) from 1990 to 2019 to collect high-quality temperature, salinity and oxygen measurements. It was imperative for the 1990-2019 BIO deep-sea oceanography missions, exclusively in this period, to maintain the 0.0010 and 0.0015 accuracies of temperature and salinity,

respectively, achieves as one of the objective of the Deep-Ocean Observation and Research Synthesis (DOORS).

AR7W was initiated as a critical line of both one-time (A1E) and repeat (AR7W) hydrography arrays of the World Ocean Circulation Experiment (WOCE). Among many other international beneficiaries of AR7W were the Global Climate Observing System (GCOS), Climate Variability (CLIVAR) component of the World Climate Research Programme (WCRP), and Global Ocean Ship-based Hydrographic Investigations Program (GO-SHIP). The AR7W observations were repeatedly used and accentuated in a number of studies aimed to quantify and understand both physical processes and full-depth ocean variability in the subpolar North Atlantic (e.g., Lazier et al. 2002; Yashayaev 2007a and 2007b; Yashayaev et al. 2007a and 2007b; Yashayaev and Dickson 2008; Kieke and Yashayaev 2015; Yashayaev et al. 2015a; Yashayaev and Loder 2009, 2016 and 2017; Chomiak et al., 2022), including high-impact publications (e.g., Dickson et al. 2002; Curry et al. 2003; Thornalley et al. 2018; Lozier et al. 2019; Fröb et al. 2017; Holliday et al. 2020; Yashayaev 2024), special journal issues (e.g., Yashayaev 2007c; Yashayaev et al. 2015b; also Yashayaev et al. 2015a; Kieke and Yashayaev 2015), books (e.g., Dickson et al. 2008), the Fourth and Fifth Assessment Reports (AR) of the Intergovernmental Panel on Climate Change (IPCC; e.g., Bindoff et al. 2007; Rhein et al. 2013), the International Council for the Exploration of the Sea's (ICES) Reports on Ocean Climate (IROC, e.g., González-Pola et al. 2020) and Northwest Atlantic Fisheries Organization (NAFO) reports (e.g., Yashayaev 2023).

The international profiling Argo float array deployed in 2002 provides real-time year-around observations all over the World Ocean, including the Labrador Sea. Other than the period of dense uninterrupted seasonal coverage of the central Labrador Sea that has been going on since 2002, owing to the International Argo Program, there was an almost decade-long period around 1970, when the Weather Ship Bravo patrols provided year-round water sample and reversing thermometer based measurements. The changes in seasonal distribution of oceanographic observations in the central Labrador Sea over seven and a half decades are depicted in Figure 2.

The steps of comprehensive quality control, problem correction, processing and integration of this and other massive oceanographic datasets were performed using computer software built, implemented and maintained by the author as part of this study (Yashayaev 2024). As part of these tasks, the Argo float and ship-based measurement are routinely edited and calibrated and projected on arbitrarily chosen transects (sections), domains (time series) and levels (maps). Figure 1a shows a special "hybrid" coordinate systems used to construct the sections plots presented and discussed later in this report. Figure 1b defines the central Labrador Sea (CLS) used for the constructions of the time series also covered in here. Figures 1c,d,e show the maps of de-seasoned de-trended salinity based on the cleaned and calibrates Argo float and ship-based profile data vertically interpolated and averaged over three vertical layers. The details of the methods used to construct the section plots, maps and time series, and other oceanographic data analyses can be obtained from the author (Yashayaev 2024).

The following four sections, *Meteorological Observations*, *Remotely-Sensed Sea Surface Temperature*, *Sea Ice Observations,* and *In-Situ Oceanographic Observations*, introduce the data sources used to produce this report, each starting with brief descriptions of respective data and methods, and present general climatological and environmental metrics obtained with these data. The seasonality in the seawater properties and its impacts on the reported ocean state variables and other general issues concerning shipboard survey data synthesis limitations are discussed in *Adequacies and Limitations of In-Situ Observations for Monitoring Interannual Changes in the Labrador Sea*. The next section, *Winter Convection and Hydrographic Conditions in the Central Labrador Sea*, provides a detailed view and discusses the mechanisms of both long- and short-term variability in the Labrador Sea. In the *Numerical Model Results* section, the past BIO North Atlantic Model results are updated to include the

year of reporting and to connect the changes in water mass characteristics and boundary current systems. The key results and Labrador Sea condition parameters are summarized in the *Summary* section.
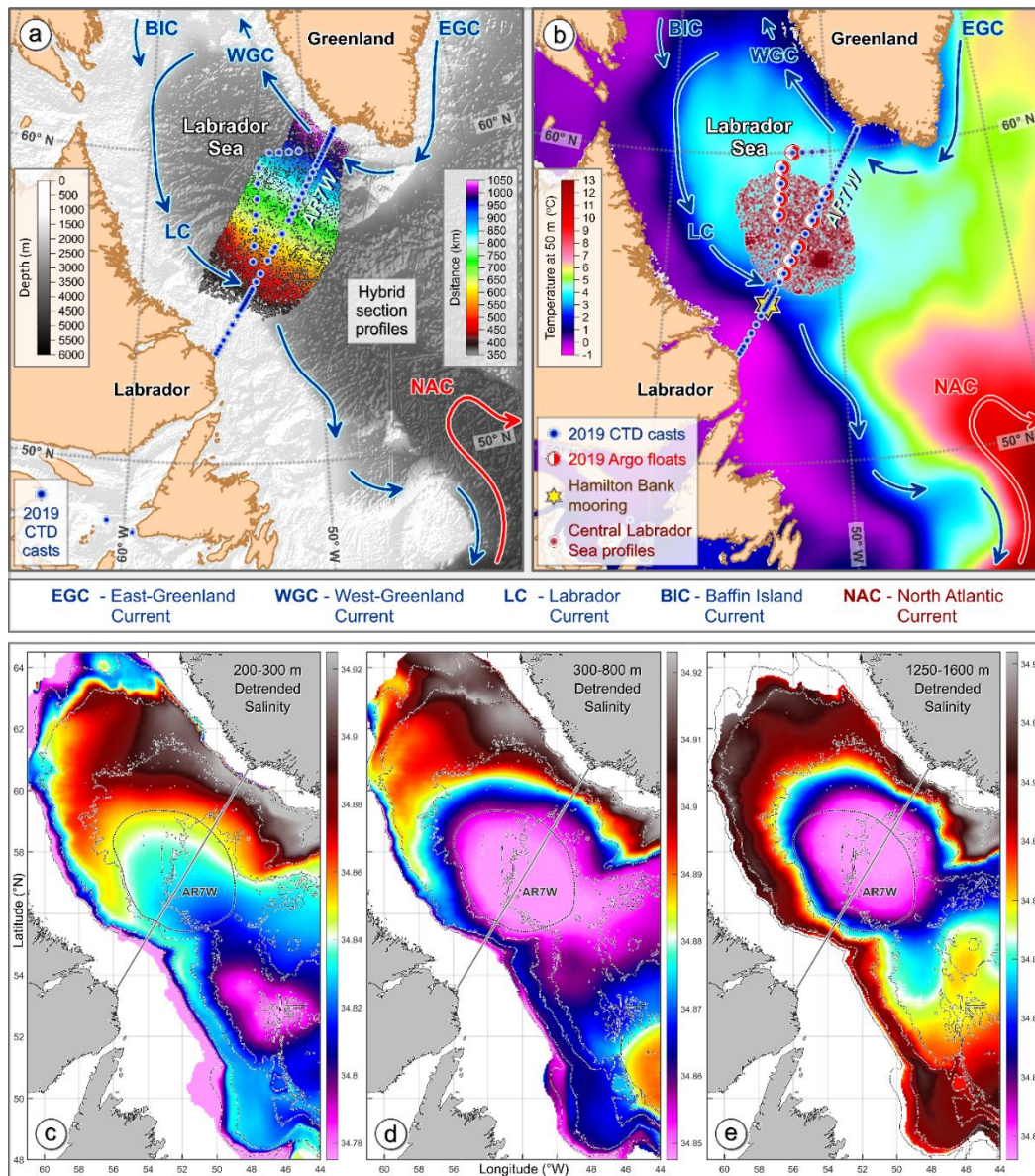

Figure 1. The key topographical features (**a**), temperature climatology at 50 m depth (**b**), and major upper currents of the Labrador Sea. The locations of the 2019 Argo float deployment (**a**), oceanographic station (**a**, **b**), and Hamilton Bank mooring (**b**; ~1000 m depth). The locations of the float and ship-based measurements used to construct the composite seawater property sections (**a**; *colour-coded by distance*) and central Labrador Sea time series (**b**; *dark red*). Maps of the de-seasoned, low-pass filtered, and averaged, first vertically over the 200-300 m (**c**), 300-800 m (**d**), and 1250-1600 m (**e**) layers, and then over overlapping spatial bins, 2002-2023 Argo float and ship-based salinity values. The Central Labrador Sea region and AR7W repeat hydrography line are indicated with black dotted and gray lines, respectively (**c–e**).Bathymetric contours are shown in the background. {*Adapted from Yashayaev 2024.*}
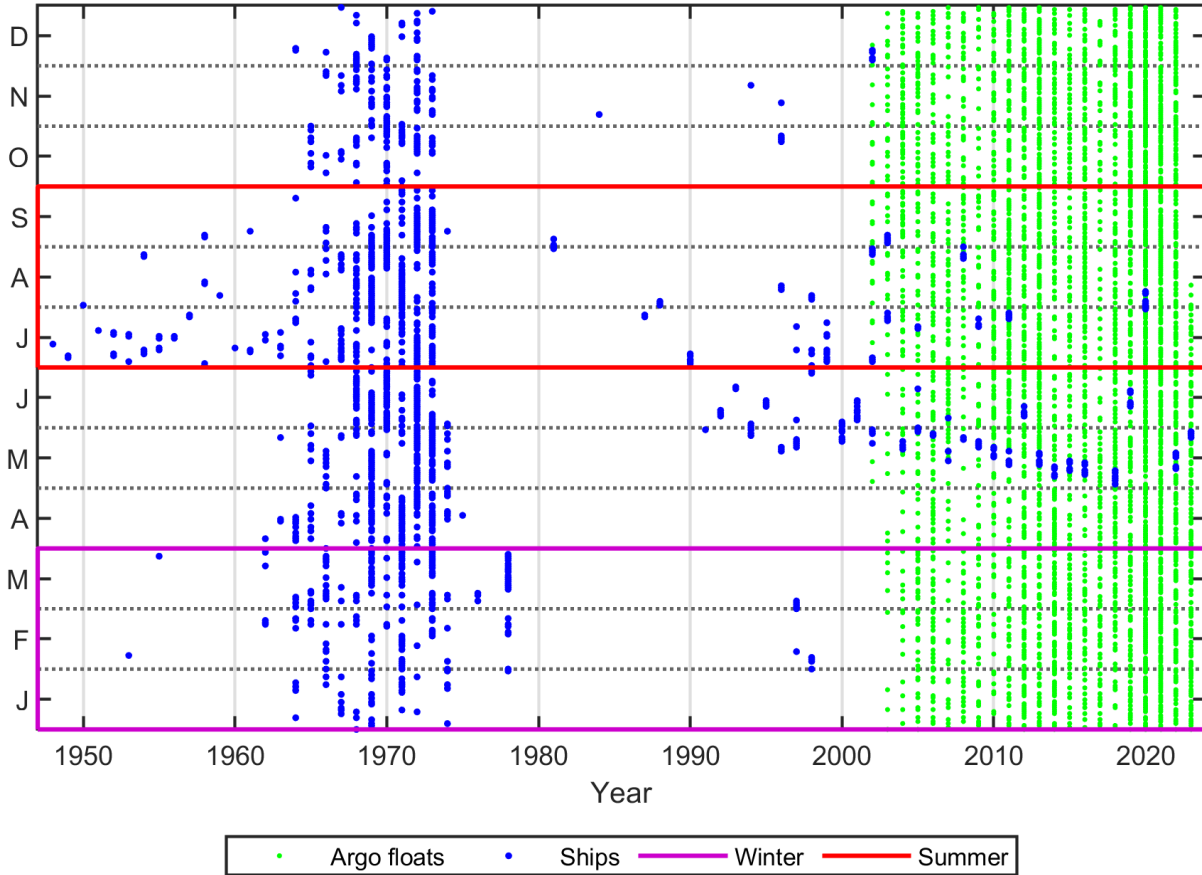
Figure 2. Seasonal (January-December) distribution of the shipboard and Argo float *hydrographic observations* collected in the central Labrador Sea (CLS) from 1948 to 2023. The CLS hydrographic observations, represented by *dark-red dots* in Figure 1 (*right*), include temperature, salinity and, in some ship surveys, oxygen.

Response of the Labrador Sea heat content to the winter atmospheric forcing

The strength, duration, and depth of winter convection in the Labrador Sea is controlled by three processes: atmospheric forcing, convective preconditioning, and post-convective restratification. Given that the winter atmospheric forcing is both initiator and lead actor of convection, we first define the metrics of its strength.

The action of the thermal winter atmospheric forcing on the water column of the Labrador Sea is depicted and explained in Figure 3 and its caption. The respective time series and their correlations are shown in Figure 4.

The ocean starts losing heat from the moment when the net (*a sum of the turbulent, such as sensible and latent, and radiative, such is incoming and outgoing shortwave and longwave, heat flux components*) cumulative (integrated forward) heat loss becomes positive, and ends when the loss reverses. The surface heat loss leads to seawater cooling that is partly compensated by the horizontal advective and diffusive heat flux from the adjacent North Atlantic basins. This understanding allows us to estimate the horizontal flux by subtracting the annual winter water-column heat content losses from the net ocean-to-atmosphere heat fluxes integrated over the respective surface cooling period (Figure 3). The start and end points of both sea-surface and water-column colling periods are defined for each winter individually.
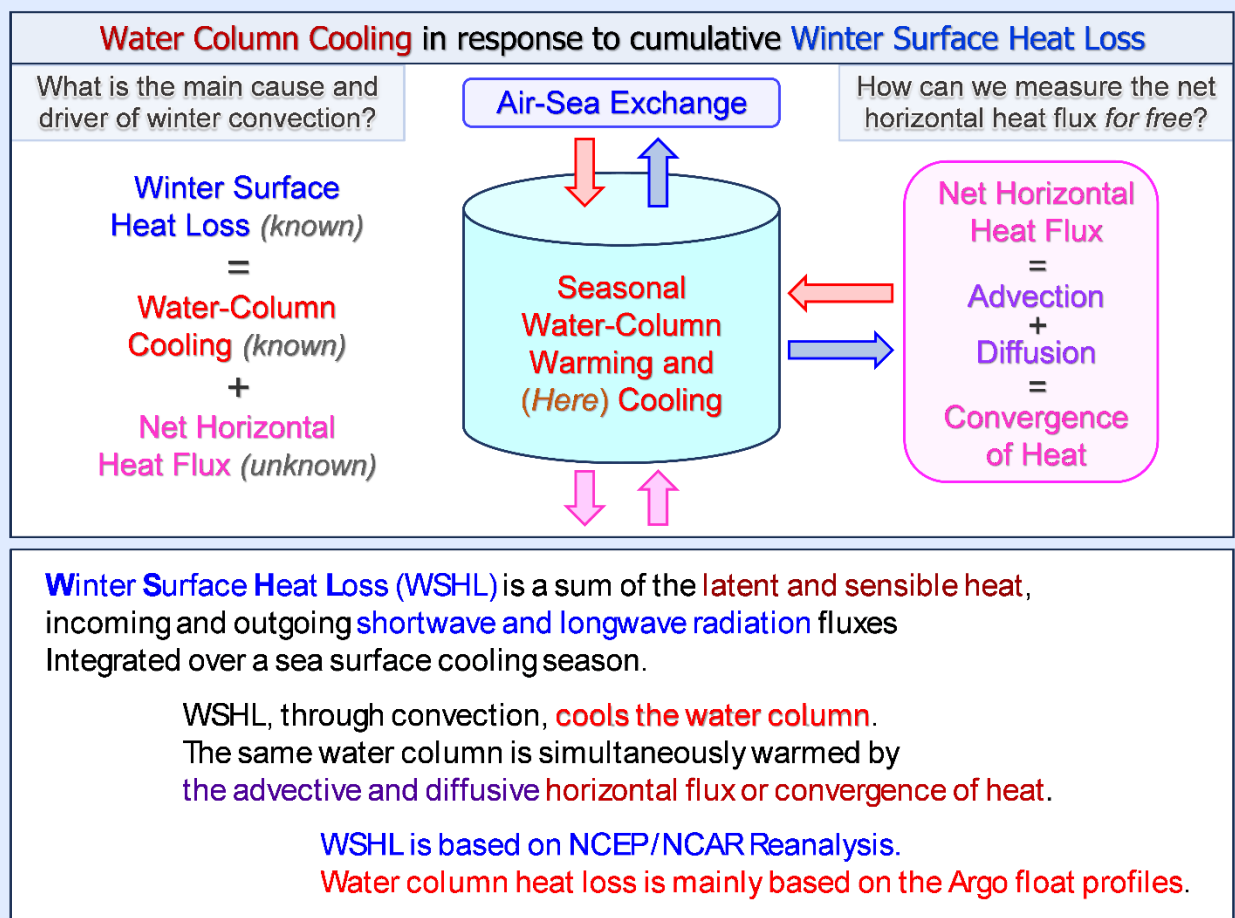
Figure 3. Schematic diagram showing the components of the CLS heat budget. In winter, the CLS water column cools due to the surface cooling imposed by air-sea heat flux (*winter surface heat loss* - WSHL). The surface heat loss is partially compensated by the net horizontal flux or convergence of heat driven by advective and diffusive processes around the CLS perimeter. The seasonal (winter) water column is estimated exclusively with the Argo data (there has not been a winter ship survey since 2002), while WSHL is based on the NCEP/NCAR reanalysis, making the two metrics fully independent with respect to the underlying data sources.

Winter surface heat loss and ocean heat content change

Winter surface heat losses (WSHL) is an amount of heat lost by the surface of the ocean (here, specifically, CLS) through air-sea heat exchange during a full cooling or winter season (Figures 3 and 4). WSHL is derived as follows.

The net surface heat flux (NSHF) values are computed for the individual time steps by adding up the incoming and outgoing shortwave and longwave radiative fluxes, and the turbulent latent and sensible heat fluxes (total of six sea-surface heat flux terms), extracted from the 6-hourly NCEP/NCAR Reanalysis fields (Kalnay et al. 1996). The spatially gridded NSHF values are then averaged over the central Labrador Sea (Figure 1, right, scattered dark-red dots).

Each cooling or winter season is identified individually in a NSHF series following the approach introduced in our earlier publications (Yashayaev and Loder 2009, 2016, 2017). Its start and end points are associated with the fall and spring NSHF sign reversals (changeovers), i.e., the moments when the sea-to-air NSHF switches to persistently positive in late fall and persistently negative in

early spring, respectively. The total or cumulative surface heat loss (WSHL) incurred by the CLS in the identified cooling period is computed by integrating the CLS NSHF from its start to end. Short-term NSHF reversals having no impact on the total heat loss are ignored.

WSHL was the highest for the 1974-2023 period in 1993 and 2015. After 2015, WSHL reduced to its ten year (2014-2023) low in 2021, and then rebounded back to above-normal in 2022, becoming the highest in eight consecutive years (2016-2023). In 2023, WSHL reduced to normal.

The total heat content losses incurred by the 15-2000 m layer of the CLS in all cooling seasons from 2002 to 2023 period are estimated in three steps: (1) a heat content time series is computed for the layer using the 2.5-day average temperature profiles (e.g., shown in Figure 6); (2) the start and end points of the layer cooling seasons are detected from respective tendency changeovers; (3) the heat content changes are integrated over the identified cooling seasons.

To better understand the action of the thermal winter atmospheric forcing, and its direct consequences, such as the impact on the Labrador Sea heat content and convection, we document three metrics characterizing the winter wind-driven mechanical atmospheric forcing. The winter heat content losses of the Labrador Sea closely follow the year-to-year changes of WSHL.

North Atlantic Oscillation (NAO) Index

The winter North Atlantic Oscillation (NAO) representing large-scale atmospheric circulation modality associated with the average subpolar North Atlantic zonal flow. The NAO is an important teleconnection pattern influencing atmospheric processes in the Labrador Sea (Barnston and Livezey 1987; Hauser et al. 2015). Under a positive NAO phase, low-pressure anomalies over the Icelandic region and throughout the Arctic, combined with high-pressure anomalies over the Azores and across the subtropical Atlantic, produce stronger-than-average westerlies across the mid-latitudes. Conditions over the northwestern Atlantic, including the Labrador Sea region, are colder and drier than average. On the contrary, a negative NAO phase indicates a relative weakening of either the Icelandic Low or the Azores High, or both, which decreases the meridional sea level pressure gradient over the North Atlantic resulting in a weakening of the westerlies and brings warmer conditions than usual. Both NAO phases are associated with basin-wide changes in the intensity and location of the North Atlantic atmospheric jet stream and storm track, and in large-scale modulations of the zonal and meridional heat and moisture transport (Hurrell 1995), resulting in the modification of the temperature and precipitation patterns. A full account of the atmospheric conditions underlying the major oceanographic developments over the past seven and a half decades (1949-2023, inclusive) is given in the *Supplementary Information* section of the paper accompanying the present report (Yashayaev 2024).

The principal component (PC)-based winter (December, January, February, March) NAO index (blue) included in this report is associated with the first empirical orthogonal function (EOF) of standardized monthly 500-mb height anomaly fields for the Northern Hemisphere. The spatial pattern of this EOF shows a high over southern Greenland, and a low near the latitude of the Azores. This index exhibits significant multidecadal variability (e.g., Figure 4, also Supplementary Figures 26 in Yashayaev 2024). After an upward trend of the NAO index from the mid-1960s to the mid-1990s there have been a downward trend to 2010, and then an increase to 2015. Recent studies reveal other atmospheric circulation patterns, which can be either complementary to NAO, (e.g., under low NAO, Hauser et al. 2015) or contribute to it (e.g., *the stratospheric polar vortex*, discussed below and in Yashayaev 2024). Further study of the atmospheric weather and climate patterns and phenomena will help to improve our understanding of atmospheric and oceanic processes and changes, and the associated predictive skills.

In 2010, the winter NAO index reached a record low (Figure 4e). In 2015, the NAO index was record high with the largest positive NAO magnitude in the 124-year-long instrumental record. Then the

NAO index experienced a decline, becoming the lowest for the last ten years (2014-2023) in 2021 and second low in 2023.

Arctic Oscillation (AO) Index

Figure 4e,f also shows the winter Arctic Oscillation index, also referred to as Northern Hemisphere annular mode, index. The AO index reflects the intensity of the tropospheric circum-Arctic circulation, possibly associated with the tropospheric polar vortex (TPV). TPV is the tropospheric counterpart of the stratospheric polar vortex (this work is restricted to the Northern Hemispheric), commonly referred to as the polar vortex (PV). PV is associated with a depression in the wintertime 50 mbar geopotential surfaces (Supplementary Figure 23 in Yashayaev 2024). TPV and PV have different sizes and seasonality – TPV is active year-round, while PV develops in winter and disappears in spring (Yashayaev 2024). Furthermore, the two have different dynamics, structures, and impacts on weather. Being largely controlled by the Icelandic and Aleutian lows, the intensity of the tropospheric polar vortex can be represented by the highly-correlated Arctic Oscillation and North Atlantic Oscillation indices (Figure 4).

North Atlantic Stratospheric Polar Vortex (PV) Index

Varying in strength, size, and position, PV influences the SPNA winter surface cooling. Since the range of PV migrations can exceed its diameter, this influence needs to be assessed exclusively over the North Atlantic. The recently introduced North Atlantic (stratospheric) PV index (Yashayaev 2024) – *the inverse 50°N-80°N meridional gradient of the 50 mbar winter geopotential heights zonally averaged over the 50°W-25°W longitude range* – meets this condition. The PV index is shown side-by-side with the other winter atmospheric forcing variables in Figure 4e,f. This index capturing changes in the stratospheric dynamics is highly correlated with winter conditions in the Labrador Sea, opening a new direction for future developments and applications.

It was recently shown that the stratospheric polar vortex may affect the strength and position of the Icelandic Low, and hence the strength and direction of the westerlies (Yashayaev 2024). The stratospheric polar vortex is associated, on average, with a single low (depression) in the 50 mbar isobaric surface. The lower the depressions the stronger the vortices. The winter atmospheric forcing in the subpolar North Atlantic was found to be connected to the intensity and position of the polar vortex through the hydrostatic balance (Yashayaev 2024). A PV intensification makes the associated geopotential height depression deeper, reducing the total airmass above the sea surface, and consequently lowering SLP. With PV positioned over the Icelandic Low, this is likely to strengthen the latter, lowering its SLP, strengthening the westerlies and increasing WSHL.

Disruptions or collapses of PV increase the underlying airmass, filling the Icelandic Low, reducing the SLP gradients, consequently weakening the westerlies. Indeed, whenever the vortex weakens, disrupts or collapses, or changes its positing moving toward Siberia, the geopotential surfaces reduce their steepness over the Icelandic Low and contribution to the meridional gradient of SLP, filling or displacing the low SLP zone. This reduces the NAO index and weakens, if not reverses, the westerly winds. On the flip side, a lower SLP in the Icelandic Low may strengthen the polar vortex by lowering its geopotential heights. In any case, following these simple hydrostatic considerations the two North Atlantic atmospheric phenomena are expected to intensify or weaken simultaneously in a large number of cases, which also explains the high correlations of PV, AO and NAO. This does not preclude the situations with unmatched stratospheric (PV) and tropospheric (AO and NAO) anomalies.

This explanation of the interaction and hydrostatic cooperation of the Polar Vortex and Icelandic Low adds to our understanding and interpretation of the low and high extreme atmospheric forcing situations. Adding to the cases analyzed in the companion paper (Yashayaev 2024), here, in Figure 5, we present a schematic diagram showing how the tropospheric (the Icelandic Low) and stratospheric

(PV) low pressure system intensify each other when overlap horizontally and weaken when come apart.
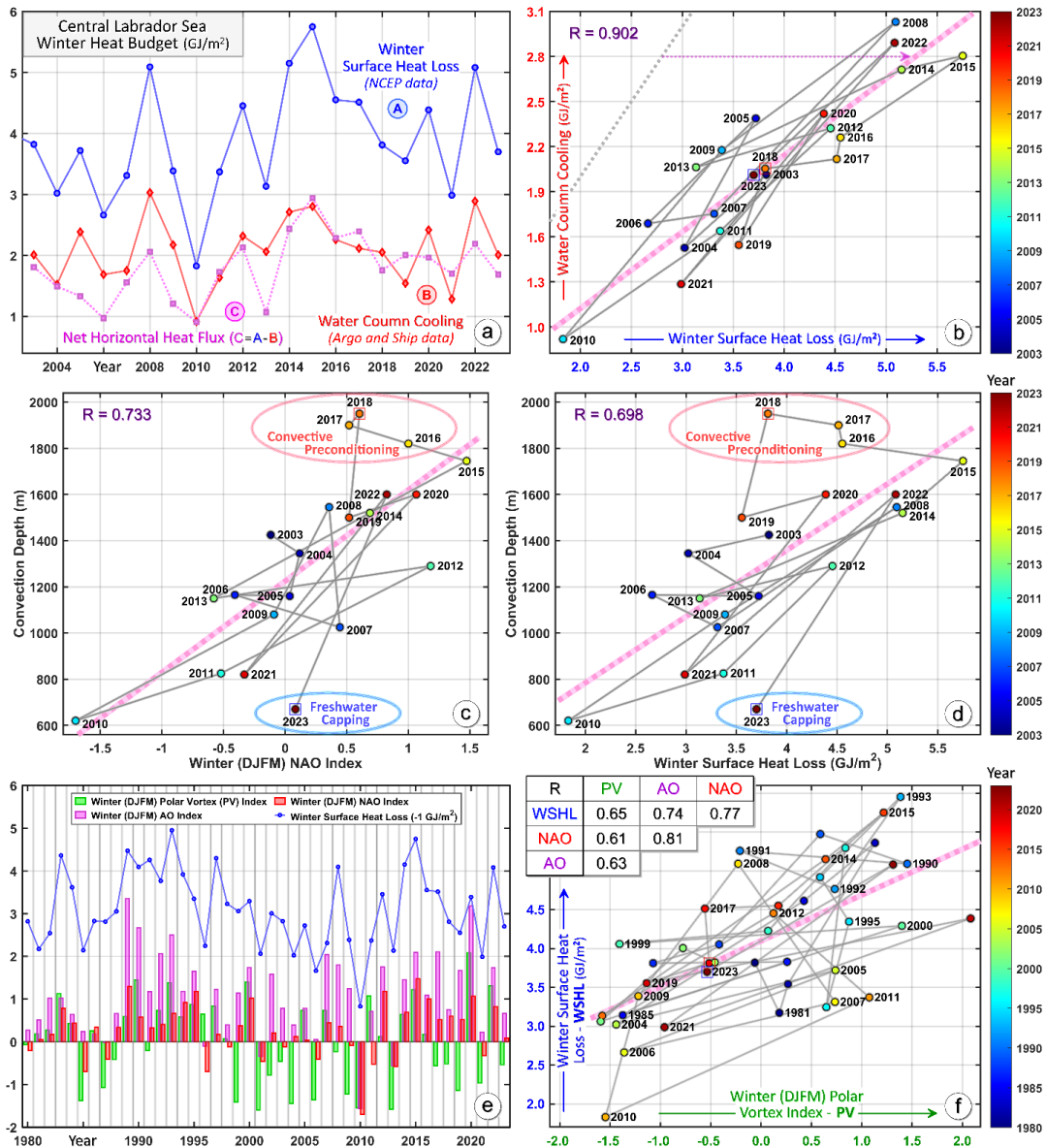

Figure 4. Metrics of the atmospheric forcing of Labrador Sea convection - how do the Labrador Sea heat content and convection depth respond to the winter atmospheric forcing? **a** The (winter) surface heat loss (WSHL) (*blue*) and 15-2000 m layer heat content reduction (*red*) computed over the individually defined respective (surface and 15-2000 m layer) cooling periods; and their difference corresponding to the horizontal heat flux (*light purple*). The horizontal heat flux is generally higher in the years with increased WSHL. **b** 2003-2023 *year-colour-coded scatter plot* of the 15-2000 m layer heat content reduction *versus* WSHL.The linear fit line (*thick pink*) diverges from the equal-value line (*gray*) supporting the statement that the horizontal heat flux (e.g., *thin pink dotted arrowed line*) increases with the ocean cooling. *Year-colour-coded scatter plots* of the convection depth *versus* the winter NAO index (**c**) and WSHL (**d**).The subpolar winter indices (**e**), the scatter of WSHL versus the winter polar vortex index (**f**).
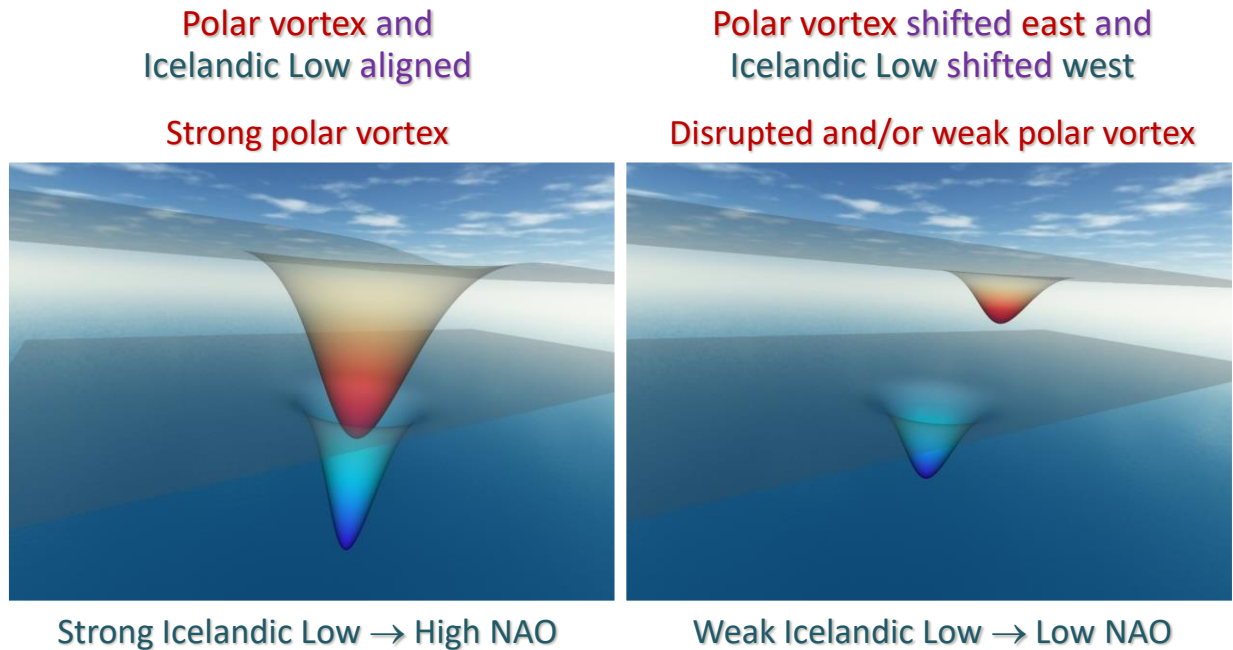
Polar vortex and
Icelandic Low aligned

Polar vortex shifted east and
Icelandic Low shifted west

Strong polar vortex

Disrupted and/or weak polar vortex

Strong Icelandic Low → High NAO

Weak Icelandic Low → Low NAO

Figure 5. Schematic diagram illustrating the interaction of the stratospheric polar vortex and the Icelandic low sea level pressure system – the Icelandic Low. When the polar vortex overlays the Icelandic Low, the airmass in the epicenter of the latter reduces consequently lowering sea level pressure in the Icelandic Low. On the contrary, when the two are located far apart, i.e., there is no or little overlap between the two, there is a larger airmass over the Icelandic Low resulting in above-normal sea level pressure.

In January of 2021 and February of 2023 PV collapsed and was mostly located east of the Icelandic Low. The PV time series (Figure 4e) show negative numbers for these years, suggesting a weak (2021) and moderate (2023) interaction with the Icelandic Low and a reduced-to-average effect on the wintertime intensification of the westerly winds. Hence, deep convection was unlikely in the winters of 2021 and 2023. However, while WSHL reached one of its record low points in 2021, it was about average in 2023, making us to expect that the depth of winter convection was also about average (~1500 m) in that year.

Synthesis of Multiplatform Oceanographic Observations

Temperature and salinity data in the Labrador Sea from various data sources are being recurrently updated, quality controlled, corrected, processed, recompiled and seasonally adjusted to build individual time series, maps, annual ocean state assessments, etc. (e.g., Yashayaev and Loder 2009, 2016, 2017; Yashayaev 2024; also the 2023 NAFO report, i.e., Yashayaev 2023). The sources of the oceanographic observations, details of data processing and analysis, and associated challenges, problems and limitations have been introduced and extensively discussed in our earlier publications (e.g., the latest, Yashayaev 2024), and NAFO (e.g., https://www.nafo.int/Portals/0/PDFs/sc/2023/scr23-038.pdf, including the *Adequacies and Limitations of in-Situ Observations for Monitoring Interannual Changes in the Labrador Sea*) and Canadian Science Advisory Secretariat (CSAS, e.g., https://waves-vagues.dfo-mpo.gc.ca/library-bibliotheque/41063478.pdf) reports on the sea conditions.

Following Yashayaev and Loder (2009, 2016, and 2017), and Yashayaev (2024), and presently including all available Argo float and ship-based observations up to the beginning of 2024 (Figure 1), time-depth series of spatially-averaged potential temperature, salinity, and potential density with weekly resolution have been computed for an area of approximately 60,000 km^2 in the central

Labrador Sea. The details of the underlying procedures from data quality control and calibration to generation of time-series can be found in the *Methods* and *Supporting Information* section   of the most recent publication (Yashayaev 2024), which encompasses the profile locations indicated in Figure 1 with the scattered pink dots, were vertically interpolated and aggregated into time series for each depth level included in a chosen layer.

Labrador Sea Convection and Water Column State Changes

Does convection always respond to changes in the winter atmospheric forcing?

The weekly composite vertical profiles of CLS temperature, salinity, density and 0.005 kg/m^3 density layer thickness (Figures 6 and 7) reveal strong seasonal cycles. Each seasonal cycle features deep winter mixing, caused by strong surface cooling (WSHL), followed by summer warming and freshening. The magnitudes and results of annual sea cooling, warming and freshening vary from year to year, often forming multiyear trends, spanning anywhere from several years to decades (Figures 6-11). We will discuss the warming and freshening parts later, starting the 2023 Labrador Sea state report with a brief overview of the recent developments of winter convection (please see our most recent journal publication (Yashayaev 2024) for a more detailed account and analysis). A water mass formed by convection is Labrador Sea Water (LSW).

Figures 6-11 reveal a recent period of recurrent intensification and deepening of winter convection spanning 2012-2018, followed by its weakening and shoaling over the subsequent years, 2019-2023, termed as convective relaxation (Yashayaev 2024). Jointly, the convective intensification and relaxation phases form a full convective cycle. We first discuss the most recent, 2012-2023, convective cycle, and then place it in the context of the longer-term convective developments. In Figure 6, LSW subscripts denote year classes.

As already noted in the *Winter surface heat loss and ocean heat content change* section and shown in Figures 4 and 10 of this report of this report, in CLS, WSHL was the highest for the entire 1994-2023 period in 2015, and the lowest for 2011-2023 in 2021. Focusing on the most recent, 2012-2023, convective cycle, we might expect that Labrador Sea convection was the deepest in 2015 and shallowest in 2021 responding to the shown year-to-year changes in WSHL. However, as we can see in Figures 6-10, the deepest and shallowest convections for this period occurred in 2018 and 2023, respectively. Hence, there must be other reasons, besides the surface forcing by cold winter air outbreaks, that contribute to progressive multiyear development and abrupt shoaling of winter convection.

Why did the deepest convection lagged the strongest surface cooling by three years?

Even though Figure 4a,b shows a high correlation (>0.9) of WSHL and cooling of the 0-2000 m water column, the convection depth shows a somewhat weaker dependence on both winter NAO (Figure 4c) and WSHL (Figure 4d). In particular, the convection depths of 2016-2018 deviated from the values predicted by linear regression. In each of these three consecutive years winter convection turned to be deeper than expected, reaching the deepest point of the entire convective cycle in 2018. The winter mixed layer, associated with a newly-formed vintage of Labrador Sea Water, was also the coldest and densest in 2018. Reaching a deeper point of convective mixing than provided by the climatological relationship between WSHL and convection depth can be explained by preconditioning of the water column by previous convective mixing events. In particular, the winter mixing events of 2012-2015 had preconditioned the water column to be susceptible to deeper convections in each of the three following years. This explains why the deepest convection of nearly three decades occurred and the moderately-strong winter atmospheric forcing conditions of 2018. By retaining the past mixed layer characteristics, convective preconditioning sustains reduced vertical stability over a vast vertical layer. This makes the preconditioning phenomenon capable of overcompensating for reduced surface cooling facilitating recurrent convective deepening.

The impact of convective precondition on the sea state can be also assessed and diagnosed using the two atmospheric forcing variables shown in Figure 10. The low-pass triangular left-side-window filtered winter NAO and WSHL series are shown in Figure 10 as purple and blue lines over the respective annual series. Each point of these lines is a weighted average of winter conditions of the current and four previous years (weights reduce linearly with time range). The NAO and WSHL left-side-window filtered values closely follow the intermediate (200-2000 m) layer temperature and density averaged annually since 1948 (regular seasonal cycle was removed from the observations prior to averaging). The agreement between the NAO and WSHL series filtered like this and annual ocean state metrics speaks for the fact that by capturing the past forcing states in the atmospheric forcing variables we account for convective preconditioning of CLS.
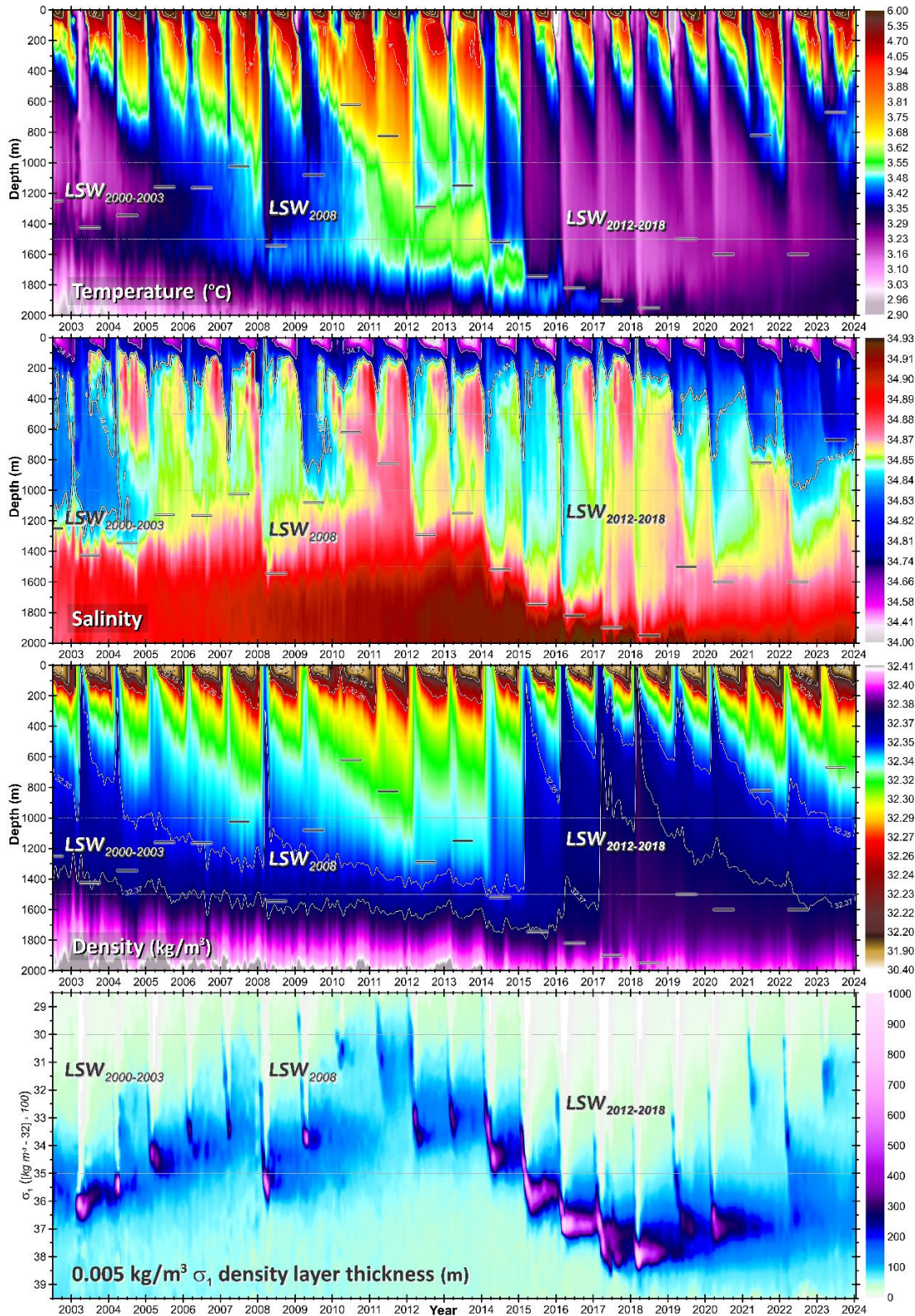
Figure 6. Central Labrador Sea temperature, salinity, density, and 0.005 kg/m³ density layer thickness based on quality-controlled and calibrated Argo float and ship-based observations. *Short horizontal lines* indicate the convection depths. *Dots* at 500, 1000 and 1500 m and 32.30 and 32.35 kg/m³ indicate the dates of the time bins.
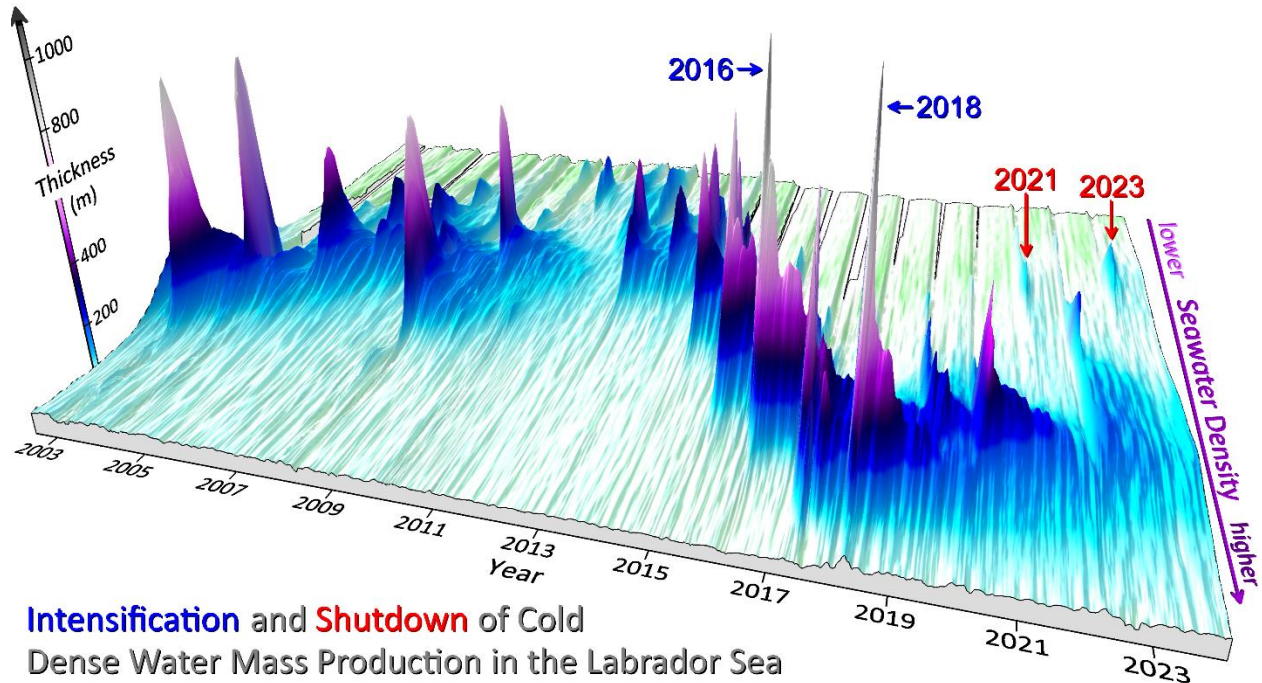
Intensification and **Shutdown** of Cold
Dense Water Mass Production in the Labrador Sea

Figure 7. 0.005 kg/m³ density layer thickness based on quality-controlled and calibrated Argo
float and ship-based observations. The values presented in this figure are analogous to
those shown in the lower panel of Figure 6. Here, the changes of density layer thickness
across the density and time bins allow us to closely follow how the most voluminous
LSW class since the 1990s developed over the 2012-2018 period, and sized to be
renewed and replenished afterwards.

Causes of the last convective relaxation of the Labrador Sea

In 2021, WSHL, strongly influenced by a disruption of the polar vortex (Figures 4 and 5), was the
lowest for 2011-2023. Labrador Sea convection responded to this decrease in winter surface colling
by shoaling from 1600 m in 2020 to 800 m in 2021. The mixed layer formed in the winter of 2021
was shallow, its temperature and density were anomalously high and low, respectively (Figure 6).

Thicknesses of overlapping 0.005 kg/m³ density range layers arranged as a function of density and
time are shown in Figure 6 (*bottom panel*), allowing to accurately define density and time of each
thickness peak, and Figure 7, placing the distribution of density range layer thicknesses in a 3D
projection to make annual water mass developments more illustrative and thicknesses easier to
compare. Once reestablished by winter convection, the thickest density layer, pycnostad, starts to
thin and transform changing all its characteristics, including density. All weekly, seasonal and
interannual transformations of the pycnostad and associated LSW properties can be easily followed
in the data compilations presented in Figures 6 ad 7. These diagrams, especially the 3D view (Figure
7) emphasize the abruptness of the recent transition from developing (2012-2018) to declining
(2019-2023) convection. Both 2021 and 2023 stand out as having extremely weak shallow winter
convection and a relatively thin mixed layer.

In 2023, WSHL was noticeably higher than in 2021 and about the same as in 2018 with the deepest
convection since the mid-1990s (due to convective preconditioning). However, in the same year
(2023), convection shoaled to a half the previous convection depth, becoming a second shallow on
record. The reason for this rapid shoaling could not be a weak atmospheric forcing, which, as just
mentioned, was near-normal in that years. The reason is obvious in the salinity time series (Figure

6) and section plots (Figure 8) showing strong freshening of the upper 600 m layer, reaching its high point in 2023 and inhabiting winter convection. The effect of this freshening on density stratification exceeded the effect of cooling at the base of the mixed layer that was much shallower than expected from the relationship shown in Figure 4c,d.
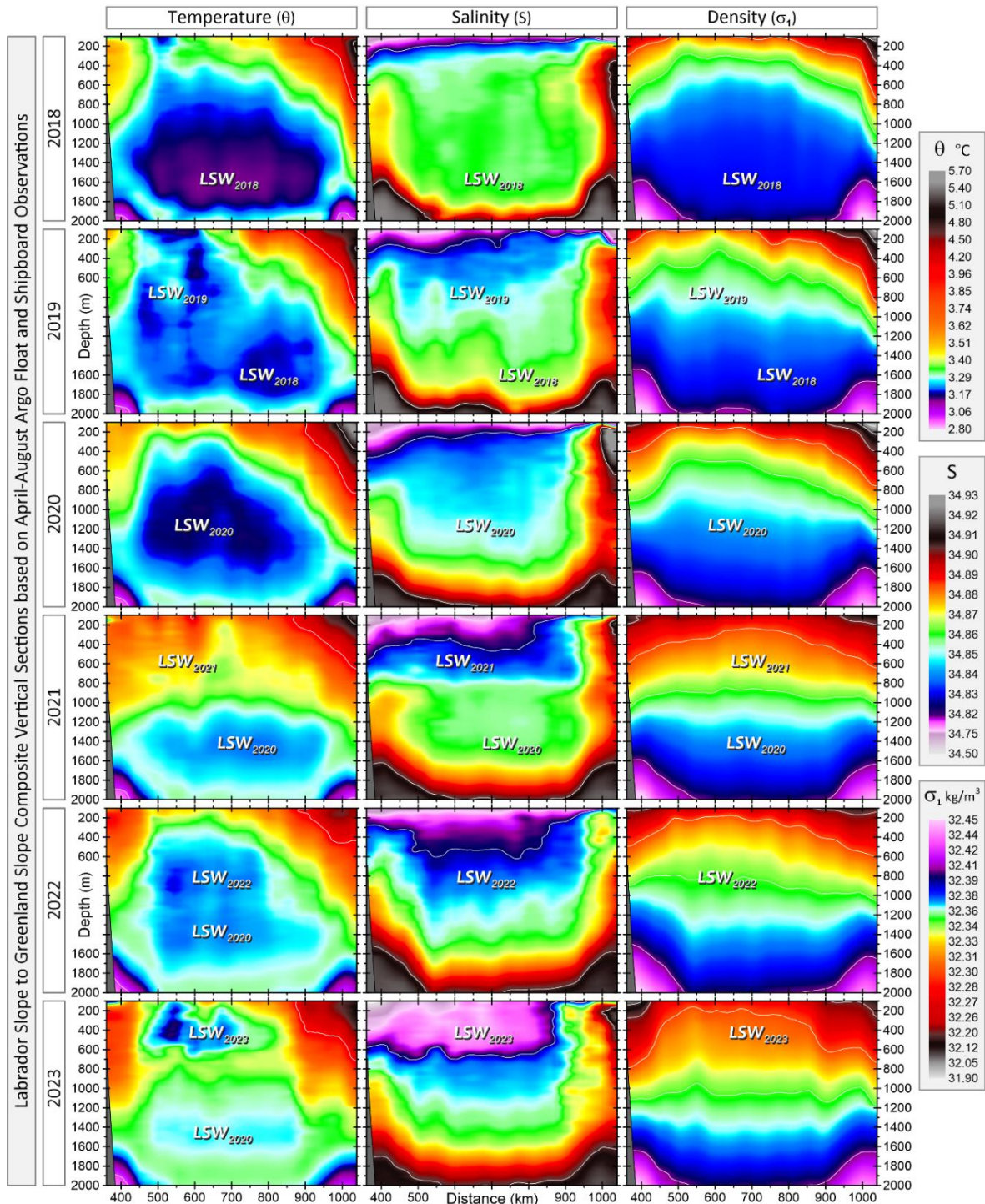

Figure 8. 2018-2023 post-convective (Apr-Aug) composite temperature, salinity, and density sections based, *mostly*, on the Argo float data, and, *to a lesser degree*, on the ship-based observations.

Multiyear convective cycles dominate decadal water property changes in the Labrador Sea

Figure 9 shows 1948-2023 progressions of full-depth annual temperature (T), salinity (S) and density profiles, and 1990-2023 annual T-S curves and dissolved oxygen progression. Time series of the annual upper, 15-100 m, and intermediate, 200-2000 m, layer properties (the seasonal cycle was removed at each vertical level prior to annual averaging), winter atmospheric forcing metrics, and Arctic sea ice extent are presented in Figure 10. Sustained multiyear cooling and freshening of the deep intermediate, 800-2000 m, layer, accompanied by accumulation of dissolved oxygen and other atmospheric gases have occurred twice since 1980, through the periods of 1987-1994 and 2012-2018 (Figure 9). These trends were similar in their duration, magnitude and transition to subsequent warming and salinification (Figure 10). Each switchover from cooling and freshening to warming and salting of the intermediate layer is imposed by a convective phase change from multiyear intensification and deepening to weakening and shoaling of winter convection (Figures 9 and 10). The last convective deepening and intermediate layer cooling were completed in 2018. The deep intermediate (800-2000 m) layer has warmed and salted since then. The largest recent changes in this layer occurred in 2021 and 2023 as shown in Figures 6-9.

How long does it take for the Arctic freshwater release anomalies to enter the Labrador Sea?

The reason for the winter of 2021 being anomalously warm giving the Labrador Sea weak and shallow convection was explained earlier in the report, but what did make the upper layer of the sea fresh in the following year causing another abrupt, and even larger than in 2021, reduction of convection depth? The likely sources of this freshening are explained in the recent publication (Yashayaev, 2024) and revisited here with Figure 11. The latter shows year-to-year progressions of the summer Arctic sea ice extent and volume (*lines*), and respective winter-to-summer change (vertical bars) anomalies.

Both summer and winter-to-summer change Arctic sea ice extent and volume anomaly series reveal three periods of extreme sea ice losses – the first two of these periods, 2007 and 2012, were year-long, while the latest one, 2019-2020, spanned two consecutive years. These sea ice losses were irreversible, meaning that there was no increase ice formation followed each loss. What this meant for the freshwater budget of the Arctic Ocean was that there were anomalously large quantities of liquid freshwater likely passing from the Arctic to the subpolar North Atlantic via Davis and Denmark straits. In the following years, the excessive quantities of freshwater were hence likely to mix in and affect the water columns along the Arctic outflow pathways. Have we seen any strong freshening events in the Labrador Sea that could be linked to the three distinctly extreme Arctic sea ice losses of the past 20 years?

Figure 11 also shows vertically and time-bin averaged Argo float ship-based CLS salinity observations that were thoroughly cleaned, calibrated and de-seasoned (*i.e., the seasonal cycle was removed, as explained later*) prior to averaging over the 15-100 m and 300-700 m vertical layers. The depth of winter convection varies year-to-year. However, the entire 300-700 m layer of CLS is likely to be left fully homogenized after every winter mixing event. For the 15-100 layer, the quality-controlled de-seasoned salinities were averaged annually, for the 300-700 m layer from April to December of each year. The winter months were excluded from the averaging performed for the 300-700 m layer. The seasonal data restriction is needed for obtaining better estimates of freshwater quantities delivered to the upper intermediate layer by convective mixing.

In the Labrador Sea, we see three events of increased freshening of the upper and upper intermediate layers over the 2004-2023 period. Basing on the low salinity occurrences in the 15-100 m and 300-700 m layers, these episodes were dated as follows: 2008-2009, 2013-2015 and 2021-2023. Remarkably the delay in the occurrences of these low-salinity states with respect to the high sea ice losses in the Arctic is on the order of 1-2 years. The record high-freshening point of the 300-700 m

layer was 2023 that, as we will see below, mostly resulted from the injecting the excessive quantity of freshwater, accumulated in CLS in the summer-fall season of the previous year, into one of the shallowest (670 m) mixed layers on record.

Yashayaev (2024) also hypothesized that the effect of the anomalous Arctic sea ice melt on the Labrador Sea was likely enhanced by the recent freshwater content stabilization/release in/from the Beaufort Gyre.
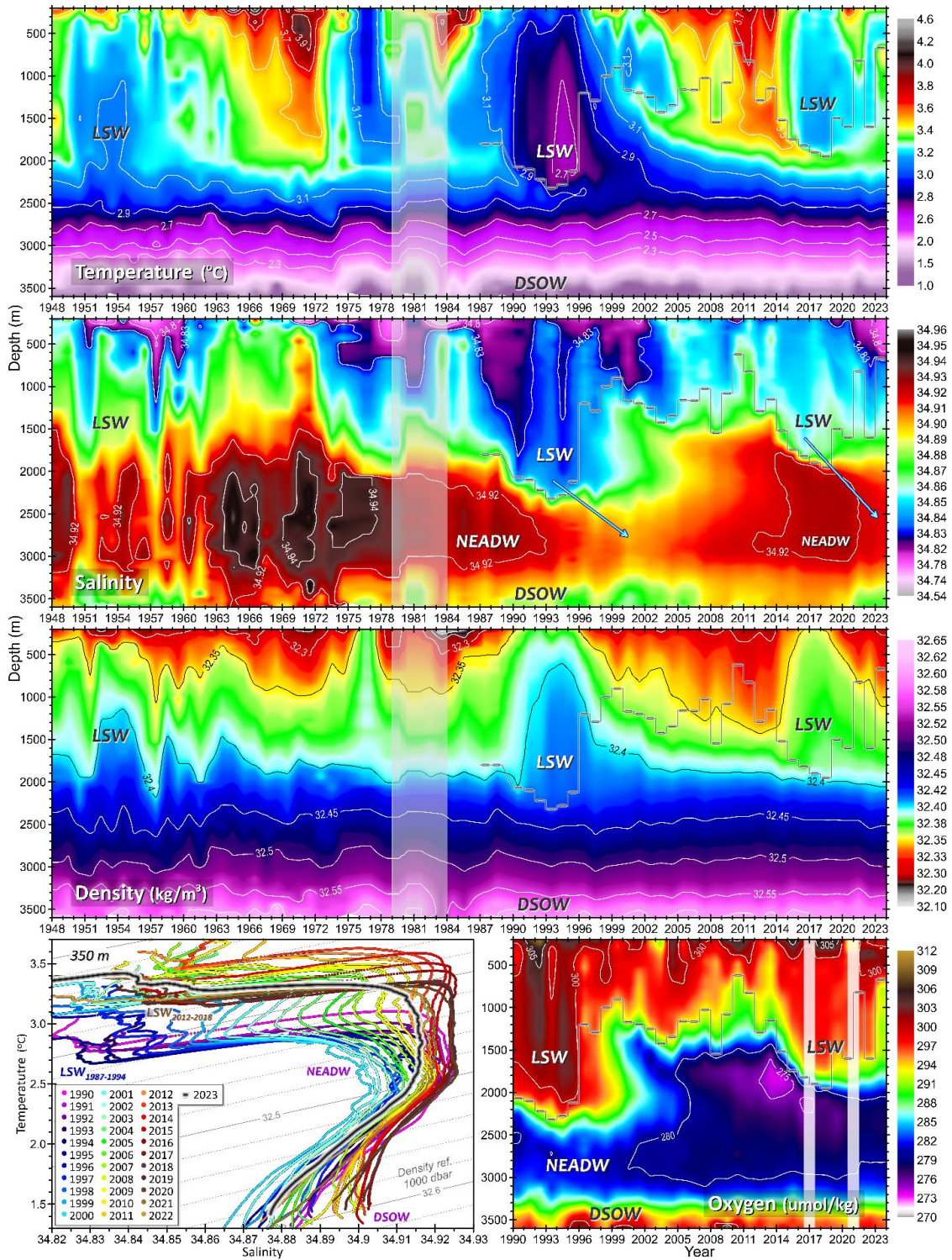
Figure 9. *Top-down:* The 1948-2023 central Labrador Sea annual temperature, salinity, and density profiles based on the edited and calibrated ship (except for 2017 and 2021) and 2017 and 2021 float observations; the 1990-2023 annual temperature-salinity curves; and dissolved oxygen profiles. LSW, NEADW, and DSOW indicate Labrador Sea Water, Northeast Atlantic Deep Water, and Denmark Strait Overflow Water, respectively. *Horizontal lines* indicate the convection depths computed for the period of sufficient hydrographic observations (1987-2023).
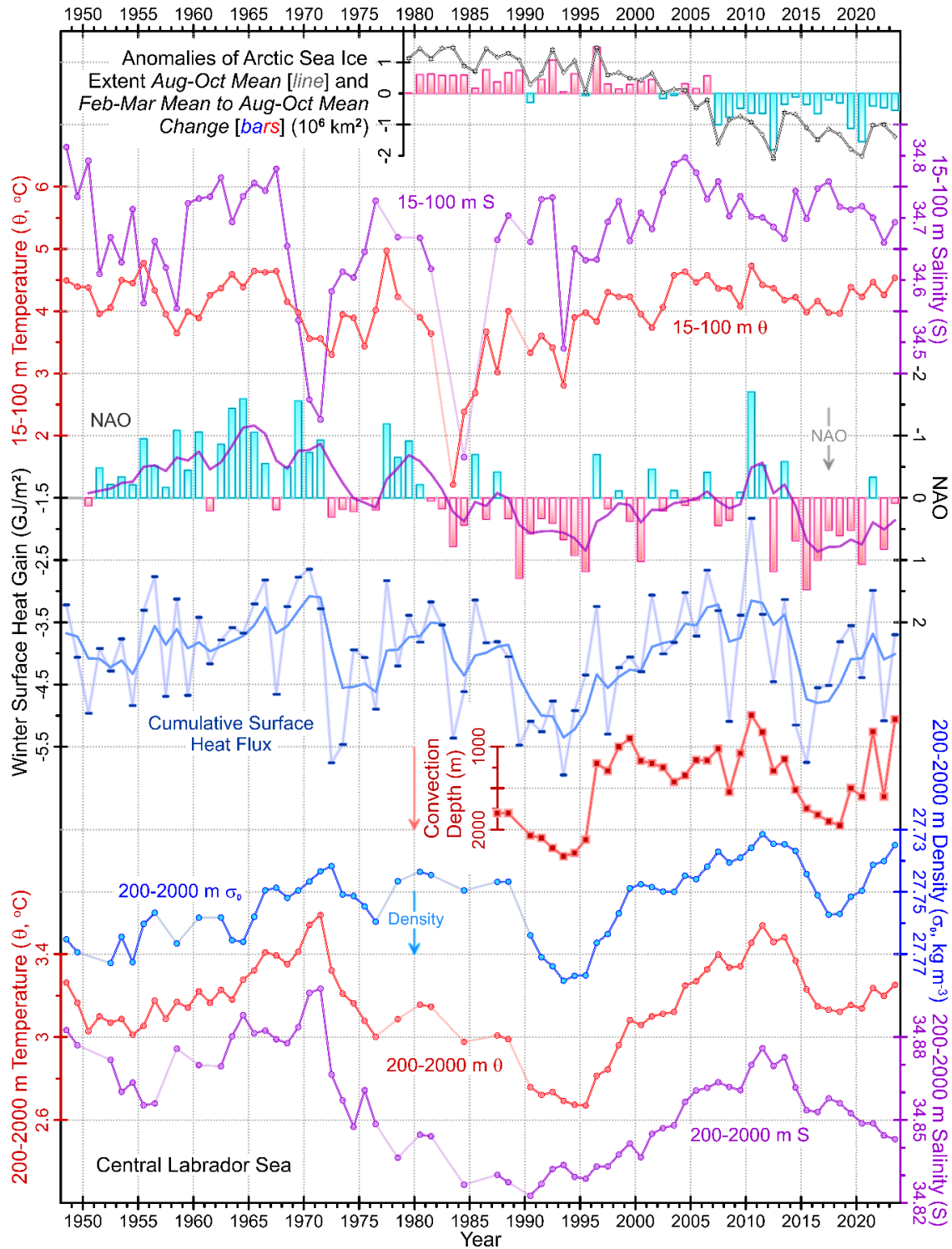
Figure 10. *Top-down*: The Aug-Oct Arctic sea ice extent, and Feb-Mar to Aug-Oct change anomalies; the central Labrador Sea (CLS) 15-100 m vertically and annually averaged de-seasoned salinity (*S*) and temperature (*θ*); the winter NAO index (*inverted*); the CLS surface heat flux integrated over individually defined cooling seasons (*blue*); the low-pass left-side-window filtered NAO and surface heat flux (*solid lines*); the convection depth; the CLS 200-2000 m vertically and annually averaged density (σ_0, referenced to 0 dbar), *θ* and *S*.
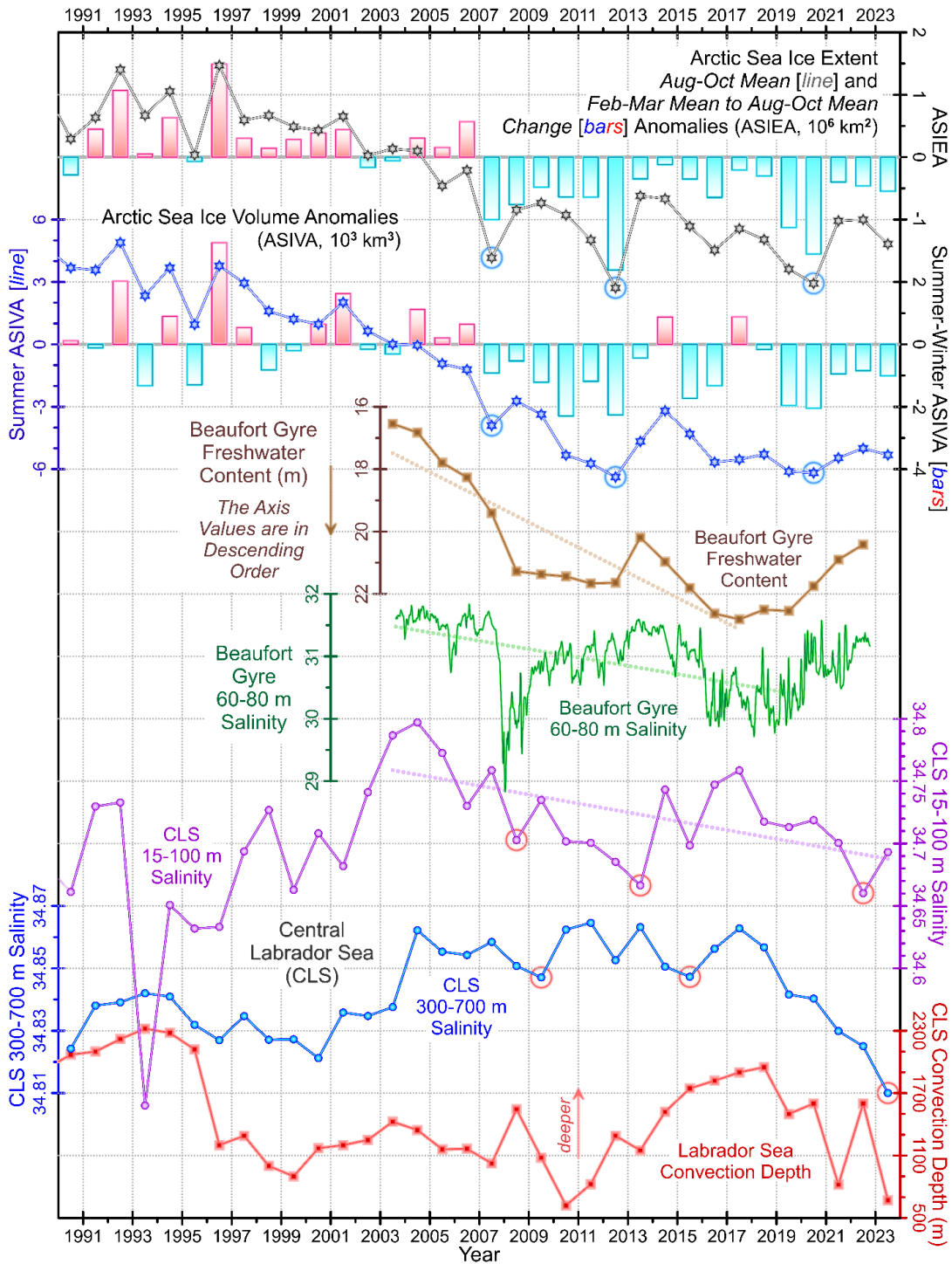
Figure 11. *Top-down*: The Aug–Oct Arctic sea ice extent and volume, and respective Feb-Mar to Aug-Oct change anomalies; the Beaufort Gyre freshwater content (m) and 60–80 m layer average salinity series based on the ship-based and McLane Moored Profiler measurements, respectively, collected as part of the Beaufort Gyre Exploration Project; the de-seasoned and averaged, first vertically over the 15-100 m layer, and then annually, central Labrador Sea (CLS) salinity, and the de-seasoned and averaged, first vertically over the 300-700 m layer, and then over the Apr-Dec period CLS salinity; the CLS convection depth.

Temperature and salinity changes in the upper layer of the Labrador Sea

Figure 12 shows temperature and salinity at 15 m depth level obtained from the individual Argo float and ship-based profiles with respect to date of profiling (decimal year) before (*dot cloud*) and after low-pass filtering with a filter window of one month (*purple-padded line*) and one year (*black line*). Figure 13 shows the same data as Figure 12, but with the seasonal cycle being removed from all individual observations as explained in the next section and in the *Appendix* section. The *dot clouds* indicate all individual measurements, *red* and *blue* from all even (e.g., 2020) and odd (e.g., 2021) years, respectively.

Figures 14 and 15 show individual temperature and salinity measurements at 15 m and 50 m depths obtained from the individual profiles depending on time of year expressed as decimal month (*1 corresponds to January 31, and 0 and 12 correspond to December 31*).

Our first statement based on the 15 m temperature series (Figures 12 and 13, *upper panels*) is that the winter and summer values are unrelated, meaning little or no persistence of anomalous signals between winter and summer and summer in winter. While the winter temperatures of the upper layer are generally correlated with convection, the summer temperatures show a different pattern of interannual changes. The most interesting part of the latter is a recurring alternation of high and low summer temperature values between the even (high temperatures) and odd (low temperatures) years during 2006-2021, except for 2018. There is no explanation of the biennial periodicity in summer temperature, and its study is underway.

In the summer of 2023, the upper layer of the Labrador Sea reached its record warm point (Figures 12-14, and A6).

As we showed and discussed before, the 300-700 m layer of the Labrador Sea was record fresh in 2023. However, this anomaly developed from the surface freshening that reached its peak in the September-October of 2022 (Figures 12-15). What we should also note when comparing the 2022 seasonal salinity signal at 15 and 50 m depths with those in the previous two years (Figures 12 and 13, *lower panels*), is that while in both 2021 and 2023, the surface (15 m) layer freshening led the freshening observed at 50 m by about two months, the seasonal minimum occurred at 15 m and 50 m at the same time in 2022. What this leads us to believe is that the origin of the anomalously low salinity signal received by the Labrador Sea in 2022 is probably different than the Labrador-Baffin shelf sea ice melt affecting the surface layer well in advance of anything deeper as obviously the case in 2021 and 2023.

The high amplitude and rate of the regular or climatological seasonal cycles (Figures 14 and 15) need to be taken into account when reporting on seasonal, interannual, decadal, and longer-term changes in the upper ocean. In the next section of this report, we discuss this aspect of data processing, analysis and interpretation in more detail.
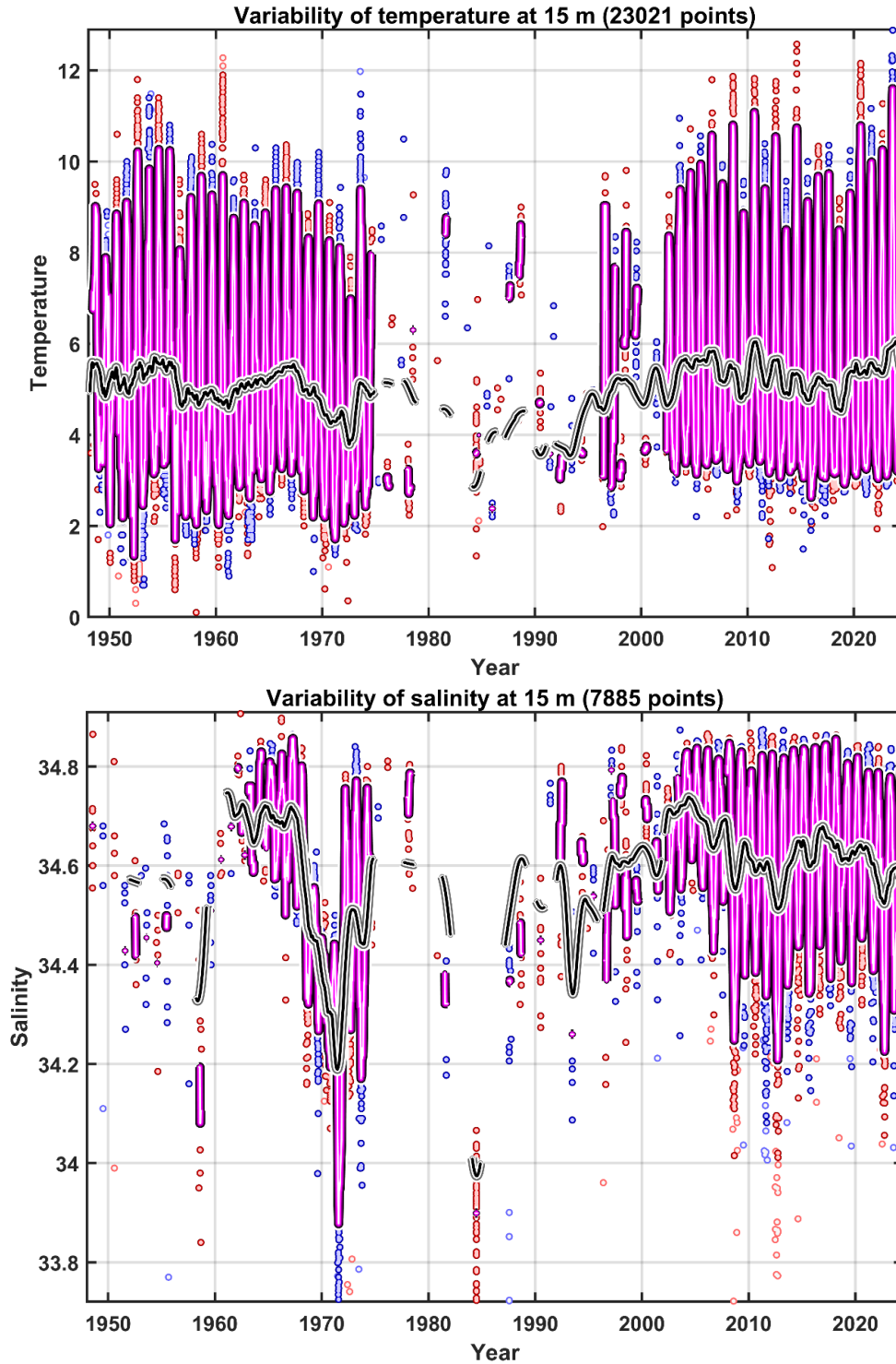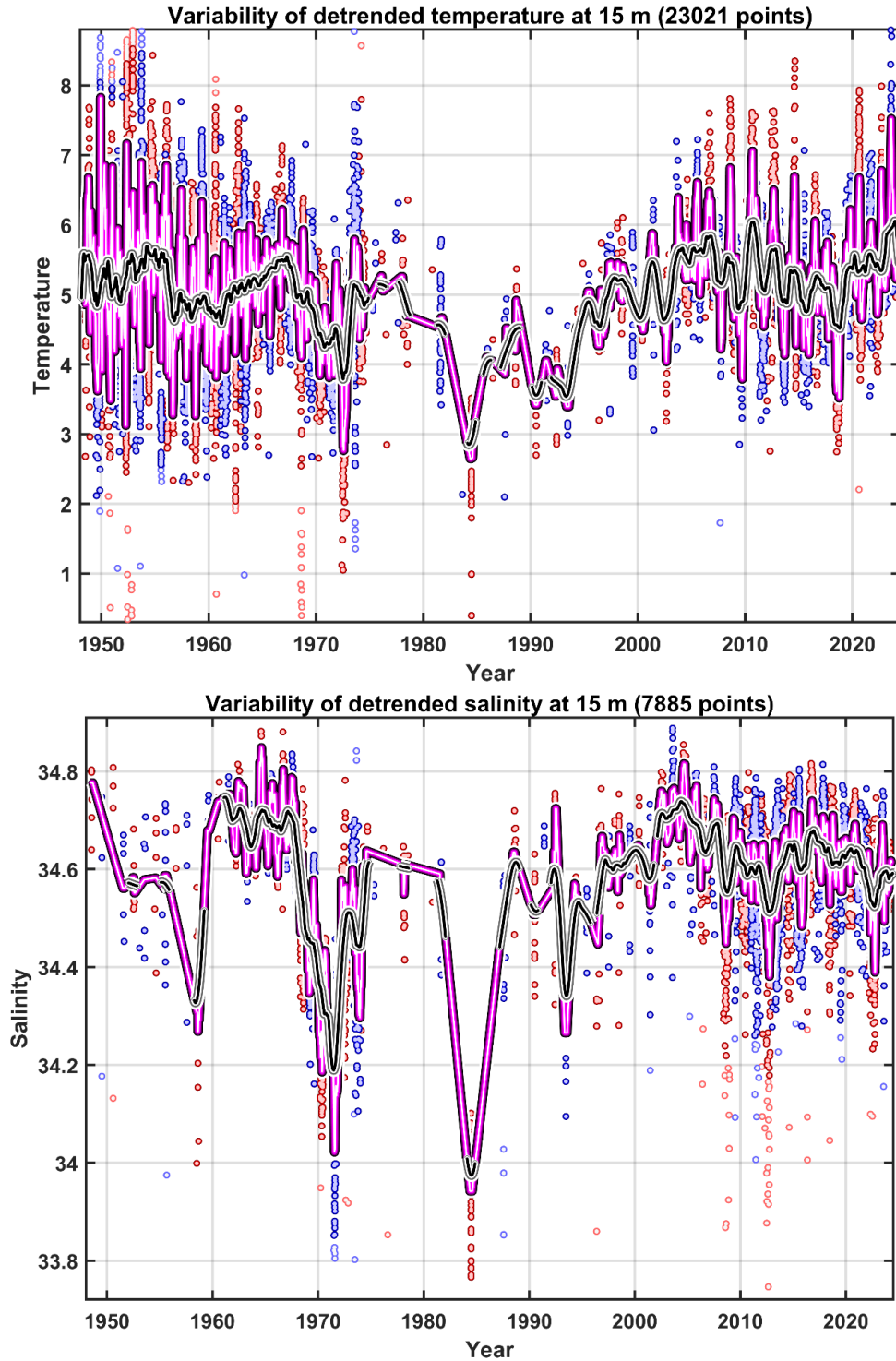
Figure 12. Temperature (*upper panel*) and salinity (lower panel) measurements at 15 m depth level in the central Labrador Sea for the period of 1948-2023 (Figure 1) with respect to decimal year. The data values for the even-numbered years (i.e., 1948, 1950, …, 2020 and 2022) are shown with *red dot clouds*, for the odd-numbered years (i.e., 1949, 1951, …, 2021 and 2023) with *blue dot clouds*. The *purple-padded* and *black lines* represents one-month and one-year low-pass filtered data, respectively.
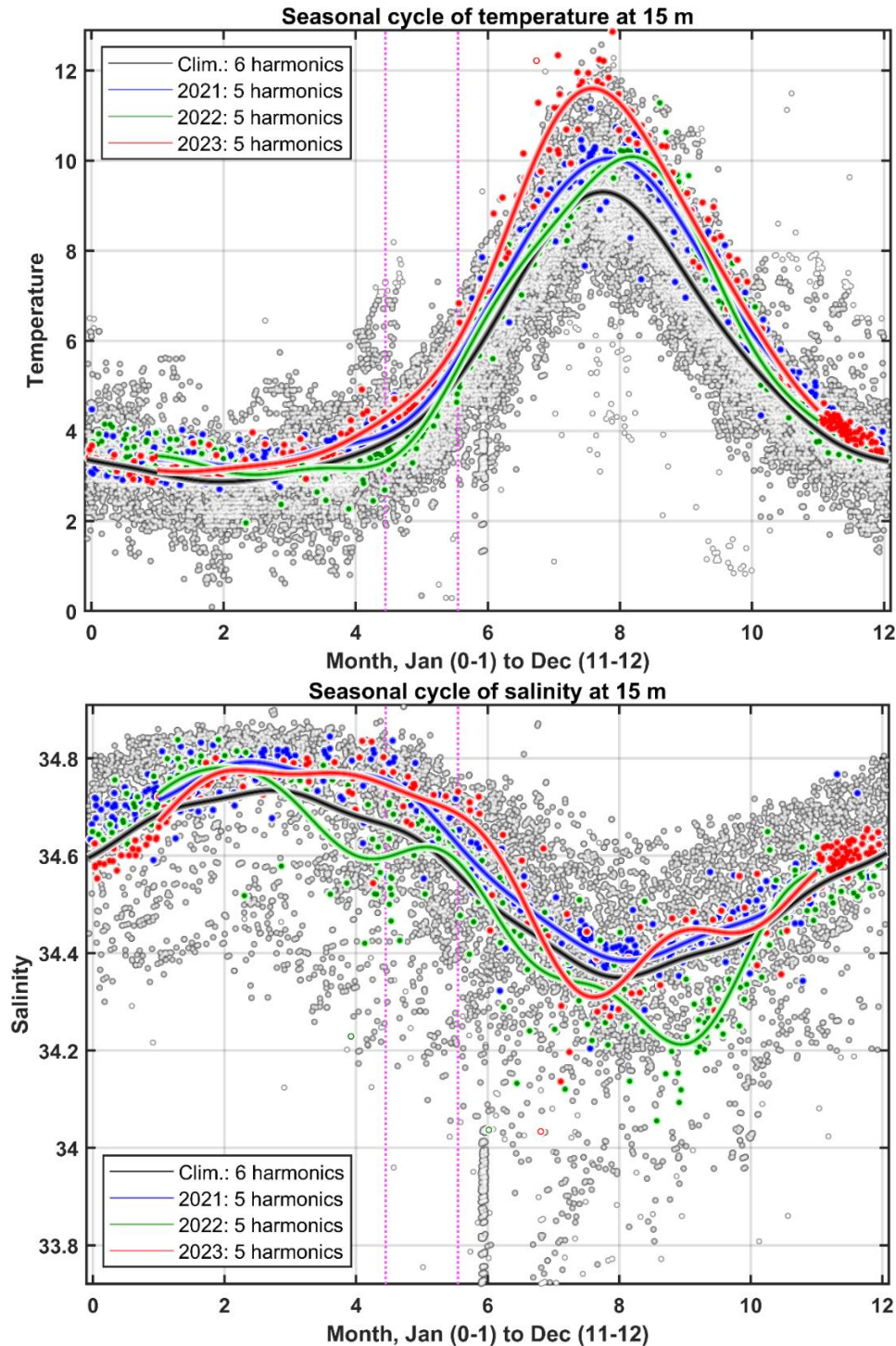
Figure 13. Temperature (*upper panel*) and salinity (lower panel) measurements at 15 m depth level in the central Labrador Sea for the period of 1948-2023 (Figure 1) with the seasonal cycle being removed from all individual observations. The data values for the even-numbered years (i.e., 1948, 1950, ..., 2020 and 2022) are shown with *red dot clouds*, for the odd-numbered years (i.e., 1949, 1951, ..., 2021 and 2023) with *blue dot clouds*. The *purple-padded* and *black lines* represents one-month and one-year low-pass filtered data, respectively.

Figure 14. Temperature (*upper panel*) and salinity (*lower panel*) measurements at 15 m depth level in the central Labrador Sea (Figure 1) for the period of 1948-2023 with respect to decimal month. The 2021, 2022, and 2023 data values, and associated seasonal cycles are shown with *blue*, *green*, and *red dot clouds*, and *lines*, respectively. The *black line* represents the all-data climatological (regular or normal) seasonal cycle. The *vertical magenta dotted lines* confine the time period from May 15 to June 15.
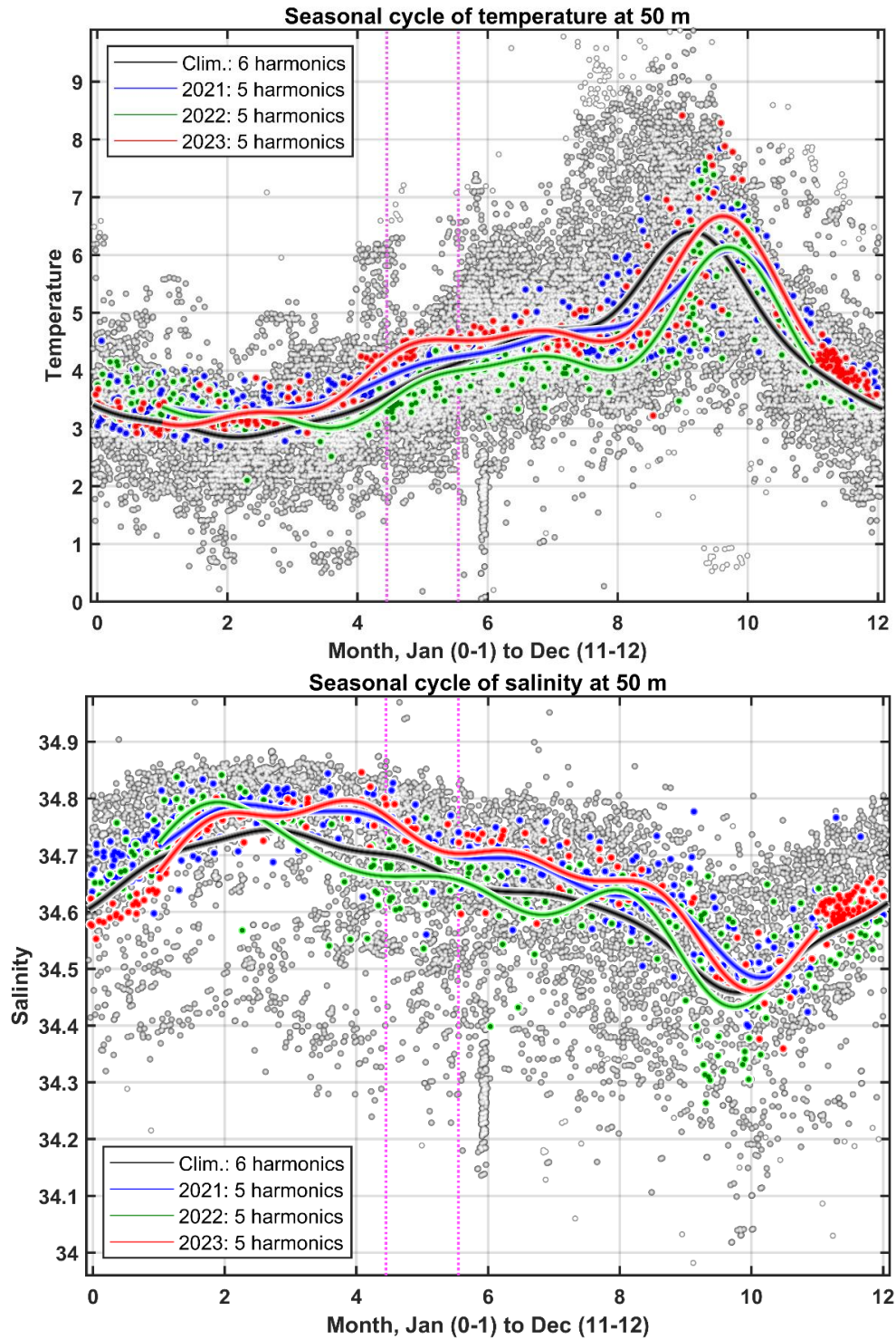
Figure 15. 1948-2023 temperature (*upper*) and salinity (*lower*) measurements at 50 m depth level in the central Labrador Sea (Figure 1) with respect to decimal month. The 2021, 2022, and 2023 data values, and seasonal cycles are shown with *blue*, *green*, and *red dot clouds*, and *lines*, respectively. The *black line* represents the all-data climatological (regular or normal) seasonal cycle. The *vertical magenta dotted lines* confine the time period from May 15 to June 15. Please note how the phase of the seasonal cycle delays with depth (here, 50 m relative to 15 m).

Why is it critically important for ocean state reporting to properly resolve the seasonal cycle?

The impacts of various limitations in data availability, spatiotemporal resolution and quality on the results and outcomes of multidisciplinary analyses, including ocean state assessments, are illustrated and discussed in our previous reports (e.g., Yashayaev 2023). Here, we revisit some aspects of the regular (climatological) and irregular (year-specific) *seasonalities* in the key oceanographic variables and accentuate why it is so important to properly resolve these signals in light of rapid and abrupt changes in the marine environment.

As shown in Figures 12, 14 and 15, and in *Appendix*, the seasonal cycle dominates the upper layer variability and remains sizeable throughout the intermediate layer (Figures 6 and 7). Given that the time series of solar radiation, and upper layer temperature and salinity are dominated by the respective seasonal cycles, and all other multidisciplinary variables are controlled or strongly influenced by these and other seasonally-active environmental variables, thorough and accurate assessments and subsequent corrections of seasonal biases in all oceanographic variables must precede any assessment of environmental condition. To achieve this goal at least one of the following conditions needs to be met:
  – *the seasonal cycle contributes to the total variance less than it does the interannual changes,*
  – *the seasonal cycle can be accurately evaluated and removed from studied observational records,*
  – *the temporal resolution and seasonal coverage of analyzed data are both sufficient and consistent.*

This requirement is based on the assessments of the regular (e.g., shown in Figures 14 and 15, and *Appendix*) and irregular or year-specific (e.g., Figures 7 and 8) seasonal cycles. *Appendix* includes the regular seasonal cycles of temperature and salinity (Figure A1), seasonal signals incurred by the upper water column over overlapping 30-day-long day-of-year ranges (Figure A2), and the seasonal gains incurred from the 15th of May onward (Figure A3). There are also the standard deviations of multiyear anomalies within overlapping 10-day bins (Figure A4), and contributions of seasonal cycles to total variances (Figure A5). The largest seasonal temperature changes are observed in April-June, at the time of the fastest increase in the solar irradiance. The noted seasonal changes exceed the interannual variability that we reported here and in the companion publications. This issue have been resolved by applying our automated procedure (e.g., Yashayaev and Zveryaev 2001; Yashayaev and Seidov 2015) to all individual observations (e.g., temperature, salinity, and density) that performs sufficient number (>25) of iterations of consecutive reevaluation of the seasonal cycle (based on harmonic approximation), removal of property value outliers, and reassessment of interannual signals. The resulting *de-seasoned* data values have been averaged annually to obtain the sough ocean state metrics (e.g., Figures 10, 11 and 13-15).

Each reporting period, such as a particular calendar year, comes with its own unique seasonal cycles in all oceanographic variables. The magnitudes, shapes, and phases of these cycles vary with location and depth, and are subject to interannual and longer-term modulations imposed on the ocean by changes in the atmospheric dynamics and oceanic heat and freshwater budgets (Yashayaev 2024). The seasonal anomalies are evaluated for each year by subtracting the regular or climatological seasonal cycle from the irregular or year-specific seasonal cycle (Figures 14 and 15). The careful evaluation of the irregularities and anomalous features, performed year by year, detection of their leading causes and consequences are all critical steps in the ocean state analysis undertaken here. Figures 14 and 15 show the individual quality controlled and calibrated Argo float and ship-based CLS observations with respect to day-of-year when those were taken, the climatological seasonal cycle (*black lines*) and 2021, 2022 and 2023 year-specific seasonal cycles (*blue, green and red lines, respectively*) at 15 m and 50 m (*any other depth and year can be analyzed analogously*).

The black lines in these figures represent the regular climatological seasonal cycle that was defined using all observations in the central Labrador Sea for the period of 1948-2022 (pink markers in Figure 1). The blue, green, and red lines in Figures 14 and 15 represent individually-defined irregular

(year-specific) seasonal cycles for 2021, 2022, and 2023. The observations used to compute the four seasonal cycles (regular and three irregular) are also shown in these figures with markers coloured in accordance with the seasonal cycle lines.

Sea Ice Observations

Sea ice concentrations derived from satellite passive microwave data since late 1978 are obtained from the U.S. National Snow and Ice Data Center. These data were used instead of the Canadian Ice Service (CIS) data because they extend farther east, so that they cover the Greenland shelf (comparisons conducted in support of this report show that the anomalies computed from each dataset for the same area agree very closely).

Monthly sea ice concentration data are used for 1978-2023 (Cavalieri et al. 1996; Fetterer et al. 2002). Ice extent is defined as the area in which ice concentration is at least 15%, and is computed for Baffin Bay, three latitude bands in the Labrador Sea region: 63-68°N (Davis Strait), 58-63°N (Northern Labrador Sea), and 53-58°N (Labrador Shelf), and the entire domain. January-through-May time series of sea ice extent anomalies for these five regions are shown in Figure 16. If in 2021 the ice extent anomalies were negative in all regions, being second record low on the Labrador Shelf, in 2022 it increased considerably to near-normal, except for Baffin Bay, and then, in 2023 decreased a bit, still remaining higher than in 2021.

It is possible that an increased sea ice extent observed in the Labrador Sea – Baffin Bay region in the winter-spring season of 2022, resulted in an increased sea-ice melt during summer, contributing to the freshening of the Labrador Sea that occurred later in the year. If combined with the extremely high Arctic sea ice losses seen in the previous years, which we expected to boost the Arctic freshwater export, this increase in sea ice melt over the Labrador Shelf and Slope might amplify the effect of the recent Labrador Sea freshening on winter convection, inhibiting it, environment and ecosystem.
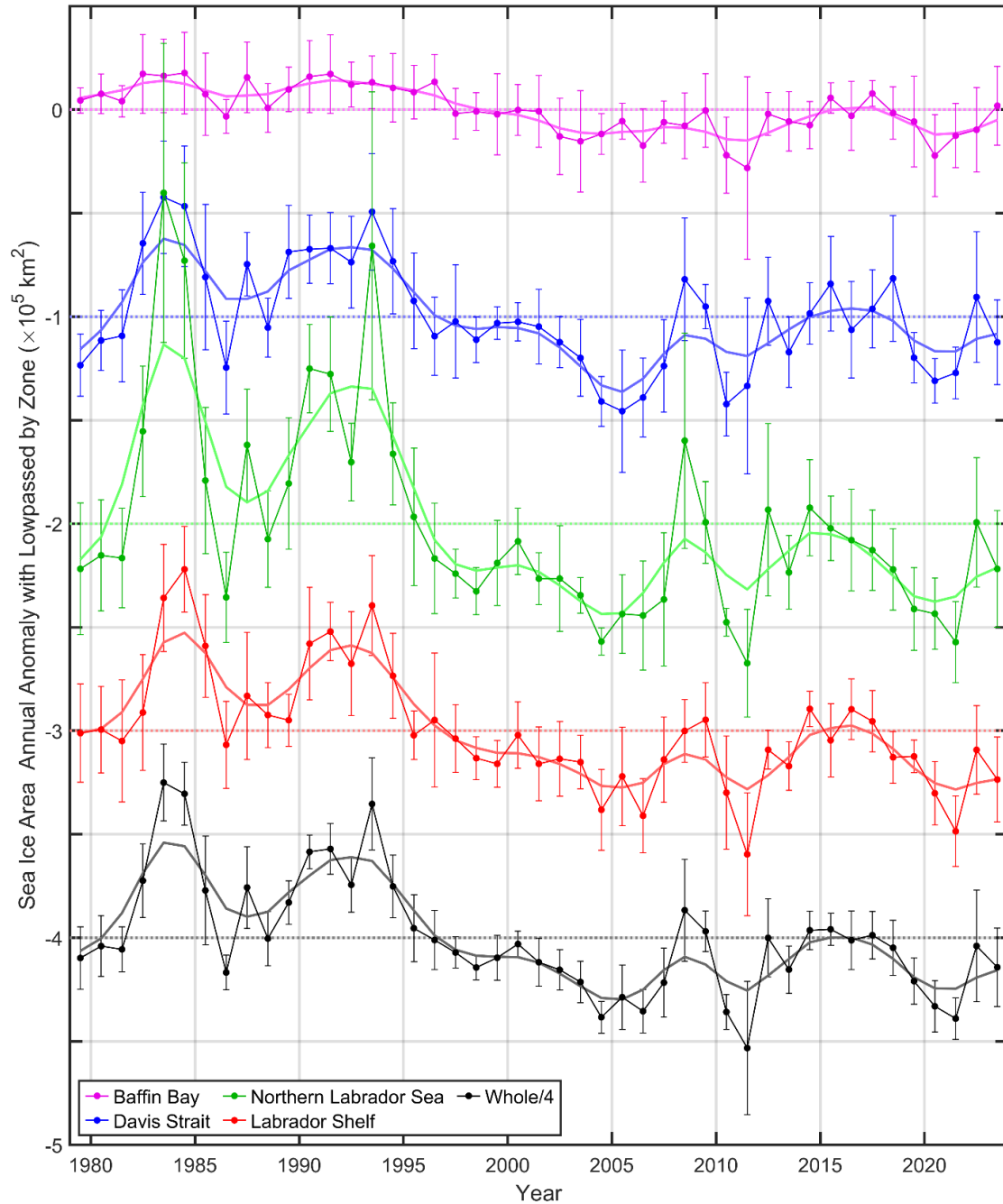
Figure 16. January-through-May averaged sea ice extent anomalies and their low-pass filtered series for Baffin Bay, three latitude bands in the Labrador Sea region: 63-68°N (Davis Strait), 58-63°N (Northern Labrador Sea), and 53-58°N (Labrador Shelf), and the entire domain, based on the US National Snow and Ice Data Center dataset. Horizontal dotted black lines represent the respective mean for the period. Vertical bars represent standard deviations.

Discussion and Conclusion

On the recent game change in the full-depth Labrador Sea state assessment and process studies

The assessments of the full-depth oceanographic conditions across the Labrador Sea, the factors determining the state of its water column, and the roles of the regional processes and water mass property trends in the North Atlantic and planetary climates are mainly based on year-round temperature and salinity profiles obtained with the Argo floats, satellite-based sea ice observations and atmospheric reanalysis data as part of the Deep-Ocean Observation and Research Synthesis (DOORS).

If before and during the World Ocean Circulation Experiment (WOCE) the seasonally-biased infrequent ship-based observations were exclusive for all full-depth ocean state reporting activities, these observations are currently integrated by the author with all other deep-sea data sources (e.g., Argo, mooring) for both data syntheses and seasonal, annual and longer-term ocean state assessments. However, the relative contribution of the ship-based data to the Labrador Sea physical state assessments and significance for the process (e.g., convection, preconditioning, restratification) studies have significantly reduced since the early years of Argo. The deep-sea data role changes can be tracked by comparing the relevant Labrador Sea publications (e.g., Yashayaev 2007a, 2007b; Yashayaev and Clarke 2008; Yashayaev and Loder 2009, 2016, 2017; Yashayaev et al., 2015a, 2015b; Yashayaev 2024) and departmental and international reports, including NAFO, of the past thirty years. Mentioning just two examples of the changing roles of various data sources in the Labrador Sea research, we should note that all of the 2017 and 2021 year-round, seasonal and annual ocean state metrics presented in Figures 4, 6-15 came entirely from Argo as there were no any ship surveys in both 2017 and 2021.

Starting from 2020 in addition to the standard Argo mission, thoroughly profiling Argo the upper 2000 m layer of the ocean, the Deep Argo mission provides year-round real-time full-water-depth temperature and salinity measurements for the Labrador Sea. We are now able to observe and analyze year-round variability of the oceanographic conditions across the Labrador Sea and resolve all seasonal processes, trends, signals and shifts at all depths. The Argo float data have replaced the ship-based observations, or merged with those available, in building the oceanographic transects (e.g., aligned with AR7W) running across the entire deep (>1000 m) basin of the Labrador Sea. This new approach to data synthesis on any predefined or arbitrary-chosen line does not depend on availability of shipboard data, and is more robust, more comprehensive, more reliable and more consistent than that based exclusively on the latter. The *Supplementary Information* section of our latest publication on Labrador Sea convection (Yashayaev 2024) includes the section plots assembled just from the ship-based observations. The multiplatform (Argo and ship) sections (Figure 8) are more appropriate for a balanced assessment of seasonal and annual oceanographic conditions.

Exploring the 2023 Labrador Sea oceanography score card

The past and recent environmental conditions in the Labrador Sea are summarized in the scorecard and presented in Figure 17. The correlations and coefficients of determination of all records included in the scorecard are shown in Figures 18 and 19. A coefficient of determination between two variables indicates the fraction of the total variance (in percents in Figure 19) explained by the linear relationship of these variables.

Important conclusions based on the scorecard: (1) The strong multidecadal signals appear in all variables, except salinity, with or without time lags; (2) The major cooling and warming events are delayed in the intermediate and deep layer relative to the atmospheric forcing, sea ice extent and upper layer (except salinity); (3) The zero-lag correlation analysis reveals groups of highly-correlated variables linked by common origin, impacts or similar responses; (4) However, the convection depth, not being strongly correlated (>0.8) with any other variable in the scorecard, is

moderately–to–moderately-highly correlated with most of the variables, signifying the aggregative or cumulative nature of Labrador Sea convection; (5) The winter atmospheric forcing variables are cross-correlated; (6) Sea ice extent shows a higher correlation with winter surface heat loss (same as negative heat gain) than with NAO and AO.
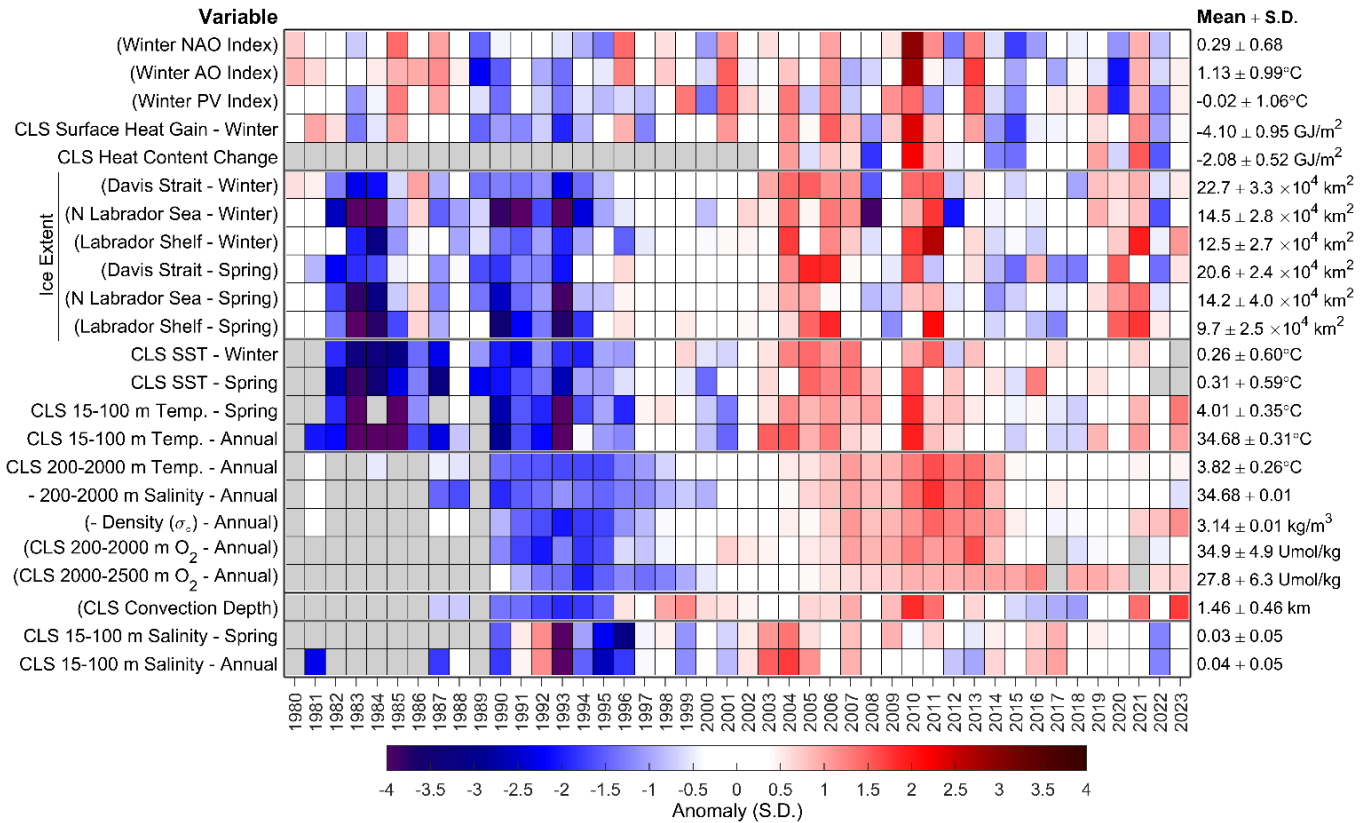

Figure 18. Scorecard of the 1980-2023 oceanographic Labrador Sea series. *Grey cells* indicate missing annual metrics; most *white cells* indicate values within 0.5 standard deviations (S.D.) of the respective long-term means for the 1991-2020 period; *red cells* indicate above normal conditions, and *blue cells* below normal. Variables whose names appear in parentheses have reversed sign and hence colour coding, whereby red cells with lower than normal values correspond to (or visually aligned with) warm conditions, and vice versa. More intense colours indicate larger anomalies. Long-term means followed by standard deviations are shown on the right-hand side of the figure. NAO denotes North Atlantic Oscillation, AO – Arctic Oscillation, CLS – central Labrador Sea, SST – sea surface temperature.
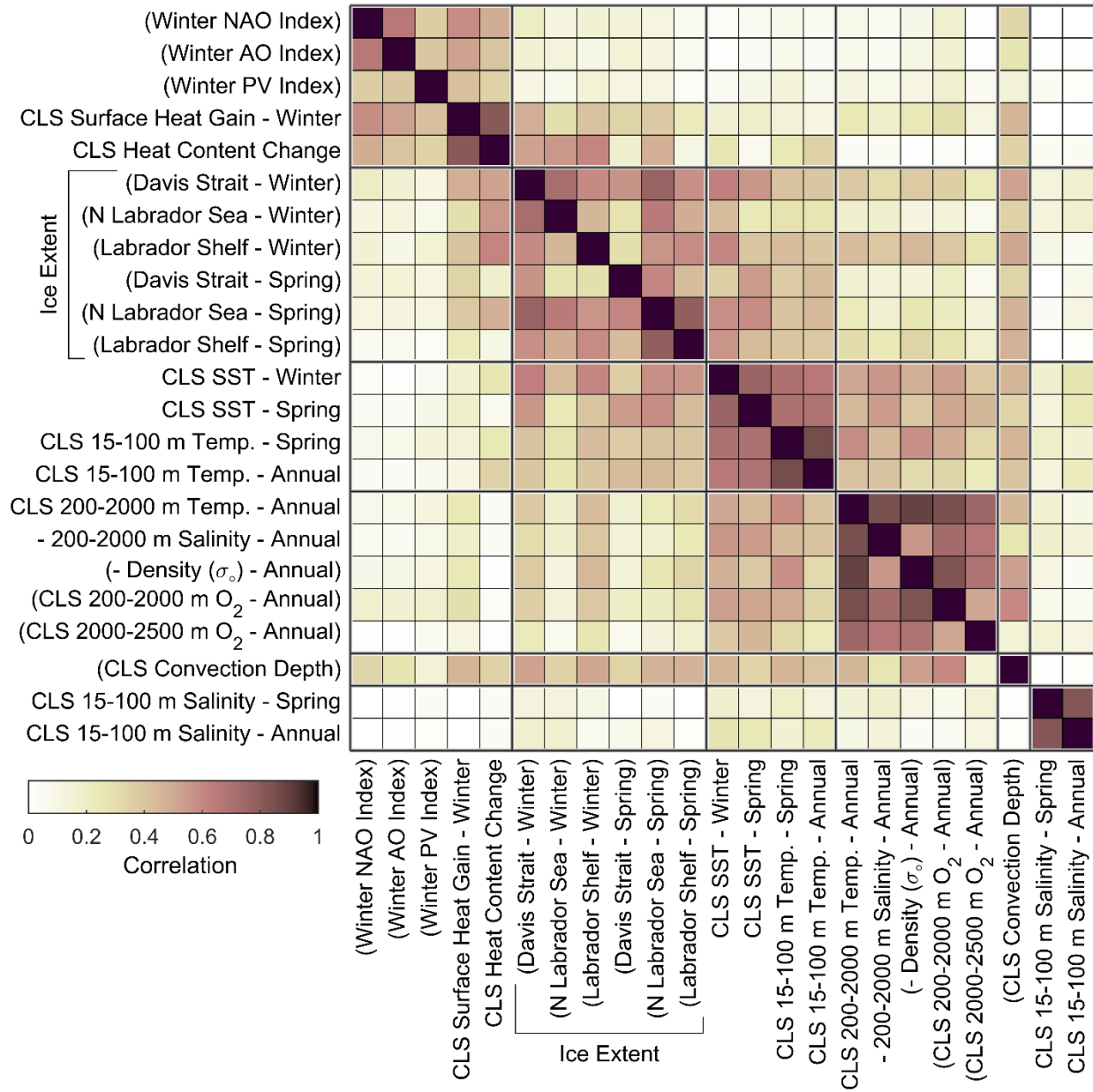
Figure 18. Correlation matrix of the time series included in the 1980-2023 Labrador Sea Deep-Ocean Observation and Research Synthesis (DOORS) scorecard. Variables whose names appear in parentheses have reversed sign, whereby all cross-correlation coefficients coloured as positive according to their unsigned magnitude. NAO denotes North Atlantic Oscillation, AO – Arctic Oscillation, CLS – central Labrador Sea, SST – sea surface temperature.
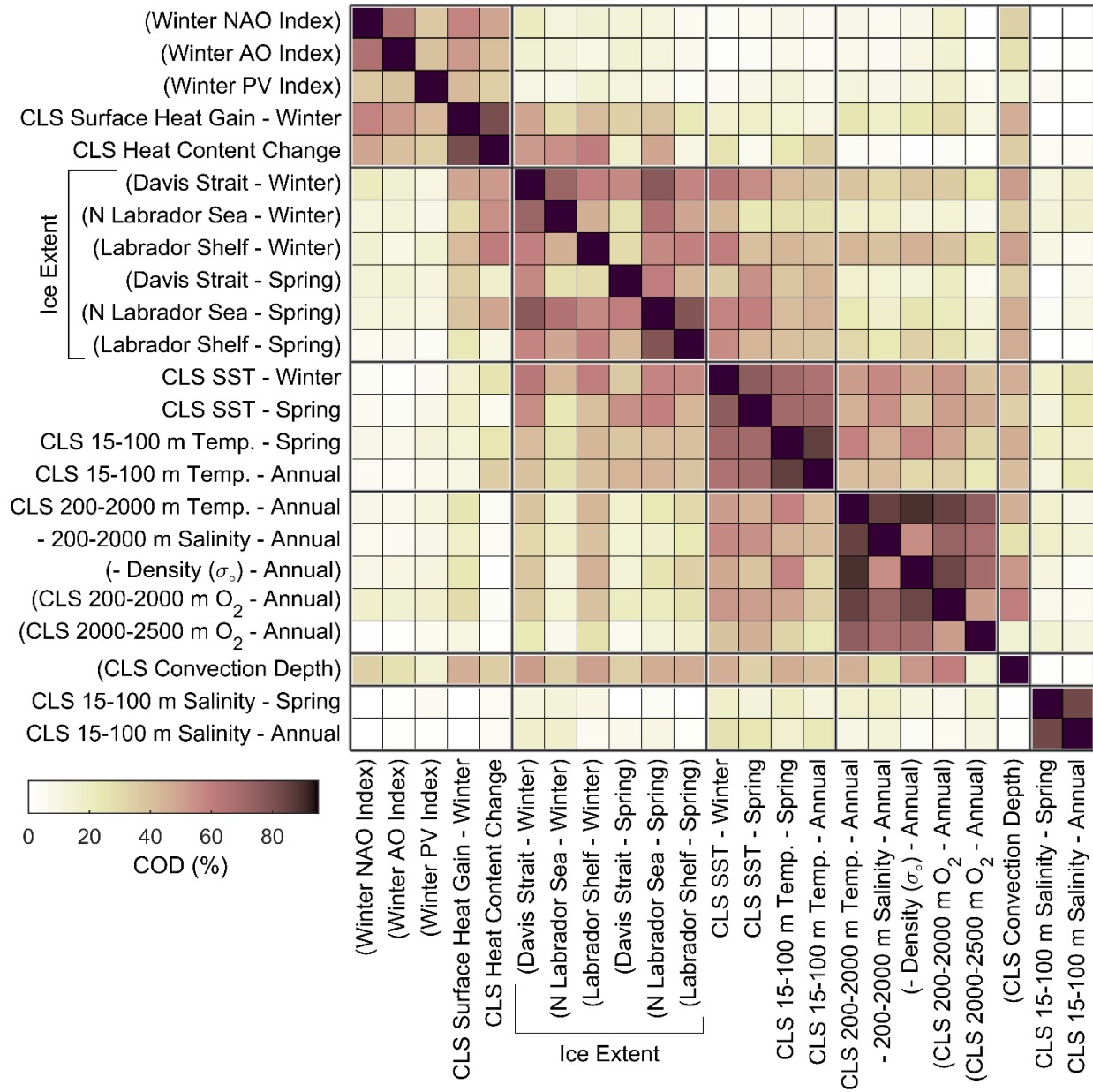
Figure 18. Coefficient of determination (COD) matrix of the time series included in the 1980-2023 Labrador Sea Deep-Ocean Observation and Research Synthesis (DOORS) scorecard. Variables whose names appear in parentheses have reversed sign, whereby all cross-correlation coefficients coloured as positive according to their unsigned magnitude. NAO denotes North Atlantic Oscillation, AO – Arctic Oscillation, CLS – central Labrador Sea, SST – sea surface temperature.

The recent convective deepening phase

Convective mixing of the Labrador Sea undergoes multi-year cycles of intensification (deepening) and relaxation (shoaling), which have been also shown to modulate long-term changes in the atmospheric gas uptake by the sea. The most recent convective cycle started in 2012, following two consecutive years of shallow winter mixing. Convection progressed deepening year by year until 2018, when it became the deepest for the entire 1996-2023 period. However, the highest winter cooling for the 1994-2023 period was in 2015, while the deepest convection occurred three years later. This time lag was due to the preconditioning of the water column by the 2012-2015 winter mixing events, making it susceptible to deep convection in three more years. The progressive deepening of winter convection from 2012 to 2018 (exceeding the depth of 2000 m in 2018) generated the largest, densest and deepest class of Labrador Sea Water since 1995.

The Labrador Sea during the convective relaxation phase

Convection weakened after 2018, rapidly shoaling by 800 m per year in the winters of 2021 and 2023 relative to 2020 and 2022, respectively. Distinct processes were responsible for these two convective shutdowns. In 2021, a collapse and an eastward shift of the stratospheric polar vortex, and a weakening and a southwestward shift of the Icelandic Low resulted in extremely low surface cooling and convection depth. It is reasoned that the collapse of the polar vortex early in that winter influenced the tropospheric pressure field and related dynamics, consequently weakening and even reversing the westerly winds over the Labrador Sea.

Global Warming has finally interrupted Labrador Sea convection

In contrast to 2021, the shoaling of convection in 2023, which turned out to be even shallower than that of 2021, and the shallowest convection for the entire 2011-2023 period, was caused by an extreme freshening of the Labrador Sea. The upper layer of the sea was the freshest since the 1990s in 2022, which lagged the extreme annual Arctic sea ice losses of 2019 and 2020 by 2-3 years. This extreme freshening entered the 300-700 m layer in 2023 through winter mixing. The two other extreme Arctic sea ice losses of the past three decades, those registered in 2007 and 2012, had been also followed by Labrador Sea freshening events.

In 2023, the central Labrador Sea experienced a near-normal cumulative surface heat loss, which was much higher than in 2021. The 2023 winter (Dec-Mar) North Atlantic Oscillation, Arctic Oscillation and Stratospheric Polar Vortex indices were also near-normal. However, in 2023, winter convection was 100 m shallower than in 2021, with below-normal winter cooling, and the shallowest since 2010, emphasising the prevailing role of freshening in control of winter convection in 2023.

The following two statements need to be taken into account to understand the significance of the recent changes to the regional climate change: (1) the recent Arctic sea ice extent and volume reductions are due to Arctic Amplification of Global Warming, and (2) in 2023, for the first time on record, the rapid shoaling of Labrador Sea convection was caused by a massive freshening of the upper layer obviously linked to the extreme Arctic sea ice loss that occurred just a few years earlier. The conclusion that follows from these statements is that Global Warming has finally entered the Labrador Sea to shoal winter convection.

The reduction in the depth of winter convection in 2023 led to a decrease in the dissolved oxygen concentration below 600 m.

Extreme upper layer temperature and 300-700 m layer salinity in 2023

With respect to temperature anomalies averaged annually over the central Labrador Sea, in the 2002-2023 period that was sufficiently covered with profiling Argo float measurements, the upper 100 m layer was the coldest in 2015 and 2018. Following 2018, this layer attained above-normal

annual men temperatures during 2019-2023, becoming the warmest for the 2011-2023 period in 2023. The 2023 summer temperature was record high.

The intermediate, 200-2000 m, layer of the Labrador Sea started to cool immediately after reaching its warmest state for the 1972-2023 period in 2011. This persistent 2012-2018 cooling trend was imposed on the intermediate layer by the progressive deepening of winter convection over the same period. The situation changed in 2019, with the depth of winter convection eventually reducing to 800 m in 2021, and then to less than 700 m in 2023. As a result, the intermediate layer has been warming since 2019. The corresponding annual density decreases contributed to a negative 2018-2023 density trend. Between 2018 and 2023, the annual mean intermediate layer density reduced by more than 0.02 kg/m³.

The freshening of the upper 100 m layer that occurred after 2017 reversed after reaching its peak in 2022. However, the 300-700 m layer continued to freshen in 2023, even showing the largest annual freshening rate ever recorded. As a result, this layer exhibited a persistent six-year, 2018-2023, freshening trend, attributed to the effect of Arctic freshwater discharge on the Labrador Sea. With respect to the intermediate, 200-2000 m, layer as a whole, the freshening trend also persisted through the same, 2018-2023, period.

Labrador shelf sea ice extent in 2023

Sea ice area from Davis Strait to southern Labrador Sea decreased between 2022 and 2023 to near-normal.

Acknowledgements

References

Bindoff, N. L., Willebrand, J., Artale, V., Cazenave, A., Gregory, J., Gulev, S., Hanawa, K., Le Quéré, C., Levitus, S., Nojiri, Y., Shum, C. K., Talley, L. D. and Unnikrishnan A. 2007. Chapter 5. Observations: Oceanic Climate Change and Sea Level, Climate Change 2007: The Physical Science Basis, Contribution of Working Group I to the Fourth Assessment Report of the Intergovernmental Panel on Climate Change, [Solomon, S., D. Qin, M. Manning, Z. Chen, M. Marquis, K.B. Averyt, M. Tignor and H.L. Miller (eds.)], Cambridge University Press, Cambridge, United Kingdom and New York, NY, USA.

Barnston, A. G., and Livezey, R. E. 1987. Classification, seasonality and persistence of low-frequency atmospheric circulation patterns. Mon. Wea. Rev., 115, 1083-1126.

Cavalieri, D. J., Parkinson, C.L., Gloersen, P., and Zwally, H.J. 1996. updated yearly. *Sea Ice Concentrations from Nimbus-7 SMMR and DMSP SSM/I-SSMIS Passive Microwave Data, Version 1*. [north/monthly]. Boulder, Colorado USA. NASA National Snow and Ice Data Center Distributed Active Archive Center. doi: https://doi.org/10.5067/8GQ8LZQVL0VL. [Accessed 08 Mar 2021]

Chomiak, L. N., Yashayaev, I., Volkov, D. L., Schmid, C., & Hooper, J. A. (2022). Inferring advective timescales and overturning pathways of the Deep Western Boundary Current in the North Atlantic through Labrador Sea Water advection. Journal of Geophysical Research: Oceans, 127, e2022JC018892. https://doi.org/10.1029/2022JC018892

Curry, R., R.R. Dickson, and I. Yashayaev, 2003. A change in the freshwater balance of the Atlantic Ocean over the past four decades, Nature, 426, 826 – 829.

Dickson, R.R., I. Yashayaev, J. Meincke, W.R. Turrell, S.R. Dye, and J. Holfort, 2002. Rapid freshening of the deep North Atlantic Ocean over the past four decades. Nature, 416, 832–837.

Dickson, R.R., Meincke, J., and Rhines, P. (Eds.). 2008. Arctic-Subarctic Ocean Fluxes: Defining the Role of the Northern Seas in Climate. 2008, Springer Science & Business Media, March 4, 2008, 736 pages.

Dukhovskoy D. S., I. Yashayaev, A. Proshutinsky, J. L. Bamber, I. L. Bashmachnikov, E. P. Chassignet, C. M. Lee and A. J. Tedstone, 2019, Role of Greenland Freshwater Anomaly in the Recent Freshening of the Subpolar North Atlantic, Journal of Geophysical Research: Oceans, Volume 124, Issue 5, Pages 3333-3360, https://doi.org/10.1029/2018JC014686.

Fetterer, F., Knowles, K., Meier, W. and Savoie, M. 2002. Updated 2011. Sea ice index. Boulder, CO: National Snow and Ice Data Center. Digital media.

Fragoso, G.M., Poulton, A.J., Yashayaev, I., Head, E.J.H., Stinchcombe, M., and Purdie, D.A. 2016. Biogeographical patterns and environmental controls of phytoplankton communities from contrasting hydrographical zones of the Labrador Sea, Progress in Oceanography, V. 141, 212–226.

Fröb, F., Olsen, A., Våge, K., Moore, K., Yashayaev, I., Jeansson, E., and Rajasakaren, B. 2016. Irminger Sea deep convection injects oxygen and anthropogenic carbon to the ocean interior, Nature Communications, 13244, doi: 10.1038/ncomms13244.

González-Pola, C., Larsen, K. M. H., Fratantoni, P., and Beszczynska-Möller, A. (Eds.). 2020. ICES Report on Ocean Climate 2019. ICES Cooperative Research Reports No. 350. 136 pp. https://doi.org/10.17895/ices.pub.7537.

Hauser, T., Demirov, E., Zhu, J., and Yashayaev, I. 2015. North Atlantic atmospheric and ocean inter-annual variability over the past fifty years – Dominant patterns and decadal shifts. Progress in Oceanography, Volume 132, March 2015, Pages 197–219.

Holliday, N.P., Bersch, M., Berx, B. et al. Ocean circulation causes the largest freshening event for 120 years in eastern subpolar North Atlantic. Nature Communications 11, 585 (2020). https://doi.org/10.1038/s41467-020-14474-y.

Hurrell, J.W. 1995. Decadal trends in the North Atlantic Oscillation: Regional temperatures and precipitation. Science, 269, 676-679.

Kalnay, E., Kanamitsu, M., Kistler, R., Collins, W., Deaven, D., Gandin, L., Iredell, M., Saha, S., White, G., Woollen, J., Zhu, Y., Chelliah, M., Ebisuzaki, W., Higgins, W., Janowiak, J., Mo, K.C., Ropelewski, C., Wang, J., Leetmaa, A., Reynolds, R., Jenne, R., and Joseph, D. 1996. The NCEP/NCAR 40-Year Reanalysis Project., Bull. Amer. Meteor. Soc., 77, No. 3, 437-470.

Kieke, D., and Yashayaev, I. 2015. Studies of Labrador Sea Water formation and variability in the subpolar North Atlantic in the light of international partnership and collaboration, Progress in Oceanography, doi:10.1016/j.pocean.2014.12.010.

Lazier, J. R. N., Hendry, R. M., Clarke, R. A., Yashayaev, I., and Rhines, P. 2002. Convection and restratification in the Labrador Sea, 1990– 2000, Deep Sea Res., Part A, 49, 1819– 1835. https://doi.org/10.1016/S0967-0637(02)00064-X

Lozier, M.S., et al., 2019. A sea change in our view of overturning in the subpolar North Atlantic, Science, Vol. 363, Issue 6426, pp. 516-521, DOI: 10.1126/science.aau6592.

Meier, W. N., Fetterer, F., and Windnagel, A. K. 2017. *Near-Real-Time NOAA/NSIDC Climate Data Record of Passive Microwave Sea Ice Concentration, Version 1*. [north/daily]. doi: https://doi.org/10.7265/N5FF3QJ6.

Progress in Oceanography, 2007, Observing and Modelling Ocean Heat and Freshwater Budgets and Transports, Edited by Igor Yashayaev, Vol. 73, 3-4, May-June 2007, Pages 203-426.

Progress in Oceanography, 2015, Oceanography of the Arctic and North Atlantic Basins, Edited by Igor Yashayaev, Dan Seidov, Entcho Demirov, Vol. 132, March 2015, Pages 1-352.

Rhein, M., S.R. Rintoul, S. Aoki, E. Campos, D. Chambers, R.A. Feely, S. Gulev, G.C. Johnson, S.A. Josey, A. Kostianoy, C. Mauritzen, D. Roemmich, L.D. Talley and F. Wang. 2013. Observations: Ocean. In: Climate Change 2013: The Physical Science Basis. Contribution of Working Group I to the Fifth Assessment Report of the Intergovernmental Panel on Climate Change [Stocker, T.F., D. Qin, G.-K. Plattner, M. Tignor, S.K. Allen, J. Boschung, A. Nauels, Y. Xia, V. Bex and P.M. Midgley (eds.)]. Cambridge University Press, Cambridge, United Kingdom and New York, NY, USA.

Rhein, M, Steinfeldt, R, Kieke, D, Stendardo, I and Yashayaev, I. 2017. Ventilation variability of Labrador Sea Water and its impact on oxygen and anthropogenic carbon: a review. Philosophical Transactions of the Royal Society A: Mathematical, Physical and Engineering Sciences, 375(2102). 20160321. doi:10.1098/rsta.2016.0321

Thornalley, D.J.R., Oppo, D.W., Ortega, P., Robson, J.I., Brierley, C.M., Davis, R., Hall, I.R., Moffa-Sanchez, P., Rose, N.L., Spooner, P.T., Yashayaev, I., Keigwin., L.D. 2018, Anomalously weak Labrador Sea convection and Atlantic overturning during the past 150 years. Nature, 2018; 556 (7700): 227 DOI: 10.1038/s41586-018-0007-4

Yashayaev, I., and Zveryaev, I. 2001. Climate of the seasonal cycle in the North Pacific and the North Atlantic Oceans. Int. J. Climatol., 21, 401-417, https://doi.org/10.1002/joc.585.

Yashayaev, I. 2007a. Hydrographic changes in the Labrador Sea, 1960-2005, Progress in Oceanography, 73 (3-4), 242-276.

Yashayaev, I. 2007b. Changing freshwater content: Insights from the subpolar North Atlantic and new oceanographic challenges, Progress in Oceanography, 73, (3-4), Pages 203-209, https://doi.org/10.1016/j.pocean.2007.04.014.

Yashayaev, I. (Ed.). 2007c. Observing and Modelling Ocean Heat and Freshwater Budgets and Transports. Progress in Oceanography. 73 (3-4): 203-426.

Yashayaev, I., Bersch, M., and van Aken, H. M. 2007a. Spreading of the Labrador Sea Water to the Irminger and Iceland basins, Geophys. Res. Lett., 34, L10602, doi:10.1029/2006GL028999.

Yashayaev, I., van Aken, H. M., Holliday, N. P. and Bersch, M. 2007b. Transformation of the Labrador Sea Water in the subpolar North Atlantic, Geophys. Res. Lett., 34, L22605, doi:10.1029/2007GL031812.

Yashayaev, I., and Dickson, R.R. 2008. Chapter 21. Transformation and Fate of Overflows in the northern North Atlantic, Arctic-Subarctic Ocean Fluxes: Defining the Role of the Northern Seas in Climate, R.R.Dickson, J.Meincke, P.Rhines (Eds.), Springer (www.springer.com), ISBN: 978-1-4020-6773-0.

Yashayaev, I., and Clarke., A. 2008. Evolution of North Atlantic water masses inferred from Labrador Sea salinity series. Oceanography 21(1):30–45, https://doi.org/10.5670/oceanog.2008.65.

Yashayaev, I., and Loder, J.W. 2009. Enhanced production of Labrador Sea Water in 2008. Geophys. Res. Lett., 36: L01606, doi:10.1029/2008GL036162.

Yashayaev, I., Seidov, D., and Demirov, E. 2015a. A new collective view of oceanography of the Arctic and North Atlantic basins, Progress in Oceanography. 132: 1-21, doi:10.1016/j.pocean.2014.12.012.

Yashayaev, I., Seidov, D., and Demirov, E. (Eds.). 2015b. Oceanography of the Arctic and North Atlantic Basins. Progress in Oceanography. 132: 1-352.

Yashayaev, I., and Seidov, D. 2015. The role of the Atlantic Water in multidecadal ocean variability in the Nordic and Barents Seas. Progress in Oceanography, doi:10.1016/j.pocean.2014.11.009.

Yashayaev, I., and Loder, J.W. 2016. Recurrent replenishment of Labrador Sea Water and associated decadal-scale variability. Journal of Geophys. Res.: Oceans, 121, 11, DOI: 10.1002/2016JC012046.

Yashayaev, I., and Loder, J.W. 2017. Further intensification of deep convection in the Labrador Sea in 2016. Geophysical Research Letters, 44, 3, DOI: 10.1002/2016GL071668.

Yashayaev, I. 2023. 2022 Oceanographic Conditions in the Labrador Sea in the Context of Seasonal, Interannual and Multidecadal Changes. NAFO SCR Doc. 23/038, N7427.

Yashayaev, I. 2024. Intensification and shutdown of deep convection in the Labrador Sea were caused by changes in atmospheric and freshwater dynamics. *Communications Earth & Environment*, 5, 156 (2024). https://doi.org/10.1038/s43247-024-01296-9

38

Appendix

Table. Oceanographic Labrador Sea cruises conducted by the Bedford Institute of Oceanography in compliance with the Deep-Ocean Observation and Research Synthesis (DOORS) or World Ocean Circulation Experiment (WOCE) temperature, salinity and oxygen data quality standards.

Cruise Name	Vessel	Project	Chief Scientist	Cruise Dates
DAW-90-012	CCGS Dawson	WOCE	John Lazier	2-Jul – 9-Jul, 1990
HUD-91-007	CCGS Hudson	WOCE	Ross Hendry	24-Apr –24-May, 1991
HUD-92-014	CCGS Hudson	WOCE	John Lazier	27-May – 15-Jun, 1992
HUD-93-019	CCGS Hudson	WOCE	John Lazier	17-Jun – 28-Jun, 1993
HUD-94-008	CCGS Hudson	WOCE	John Lazier	24-May – 12-Jun, 1994
HUD-95-011	CCGS Hudson	WOCE	John Lazier	7-Jun – 5-Jul, 1995
HUD-96-006	CCGS Hudson	WOCE	John Lazier	10-May – 2-Jun, 1996
HUD-96-026	CCGS Hudson	WOCE	Allyn Clarke	15-Oct – 20-Nov, 1996
HUD-97-009	CCGS Hudson	WOCE	Allyn Clarke	9-May – 12-Jun, 1997
HUD-98-023	CCGS Hudson	WOCE	John Lazier	22-Jun – 10-Jul, 1998
HUD-99-022	CCGS Hudson	WOCE	Allyn Clarke	27-Jun – 14-Jul, 1999
HUD2000009	CCGS Hudson	WOCE	Allyn Clarke	20-May – 8-Jun, 2000
HUD2001022	CCGS Hudson	WOCE	Allyn Clarke	30-May – 15-Jun, 2001
HUD2002032	CCGS Hudson	WOCE	Allyn Clarke	23-Jun – 19-Jul, 2002
HUD2002075	CCGS Hudson	Climate	Erica Head	29-Nov – 12-Dec, 2002
HUD2003038	CCGS Hudson	Climate	Allyn Clarke	13-Jul – 4-Aug, 2003
HUD2004016	CCGS Hudson	Climate	Allyn Clarke	14-May – 30-May,
HUD2005016	CCGS Hudson	Climate	Allyn Clarke	27-May – 7-Jun, 2005
HUD2006019	CCGS Hudson	DOORS	Ross Hendry	24-May – 8-Jun, 2006
HUD2007011	CCGS Hudson	DOORS	Ross Hendry	10-May – 29-May,
HUD2008009	CCGS Hudson	DOORS	Glen Harrison	20-May – 4-Jun, 2008
HUD2009015	CCGS Hudson	DOORS	Glen Harrison	18-May – 1-Jun, 2009
HUD2010014	CCGS Hudson	DOORS	Glen Harrison	13-May – 30-May,
HUD2011009	CCGS Hudson	DOORS	Igor Yashayaev	6-May – 29-May, 2011
MLB2012001	CCGS M.L. Black	DOORS	Igor Yashayaev	25-Jun – 20-Jul, 2012
HUD2013008	CCGS Hudson	DOORS	Igor Yashayaev	4-May – 28-May, 2013
HUD2014007	CCGS Hudson	DOORS	Igor Yashayaev	2-May – 26-May, 2014
HUD2015006	CCGS Hudson	DOORS	Igor Yashayaev	1-May – 26-May, 2015
HUD2016006	CCGS Hudson	DOORS	Igor Yashayaev	30-Apr – 24-May, 2016
HUD2018008	CCGS Hudson	DOORS	Igor Yashayaev	25-Apr – 20-May, 2018

| AMU2019001 | CCGS Amundsen | DOORS | Igor Yashayaev | 2-Jun – 19-June, 2019 |

The impact of the regular seasonal cycle on ocean state assessments based on limited observations

Figures A1-A5 show the regular seasonal cycles of temperature and salinity (A1), the associated seasonal changes occurring over 30-day day-of-year ranges (A2) and seasonal changes measured from the 15th of May (A3), standard deviations of anomalies in 10-day bins (A4) and contributions of the seasonal cycles to the total variances (A5). The estimates included in these figures are based on iterative evaluation of seasonal cycle using irregular data analysis routines (Yashayaev and Zveryaev 2001).

The regular seasonal cycle contributes to observations randomly taken within a matching 30-day-long day-of-year periods of different years. The seasonal signal encountered over each 30-day period is computed by taking the difference of its end and start values. This calculation is performed for all yeardays. Figure A2 shows regular seasonal changes of temperature and salinity over respective 30-day periods, day-by-day. The magnitudes of the seasonal changes that occur over such overlapping 30-day day-of-year ranges is the highest at the sea surface and reduces with depth. This analysis convincingly shows that any uncorrected seasonal bias entering both annual and seasonal sea state estimates with measurements randomly taken within a targeted 30-day seasonal time frame, especially if occurring in spring or fall, is likely to exceeds the magnitude of interannual changes in the upper 100 m layer (e.g., standard deviation shown in Figure A4). In particular, the seasonal warming that occurs over the 30-day period coinciding with May is much larger than the standard deviation of temperature anomalies, meaning that the seasonally-imposed scatter would be large, if a time series was constructed for the upper 100 m layer without applying a seasonal correction. Furthermore, the trend in survey date (Table) would lead to a systematic seasonal bias in a long time series forming an artificial trend, if the seasonal was not properly removed from the observations.

The contribution of the regular (climatological) seasonal cycle to the total variability is computed by dividing the variance of the estimated seasonal cycle by the total variance and multiplying the result by 100%. Figure A5 shows how this quantity changes for central Labrador Sea temperature and salinity with depth. At the sea surface, 90% of the total temperature variance is attributed to the regular seasonal cycle. The contribution of the seasonal cycle below 200 m is less than 40% for temperature and less than 20% for salinity. In both cases, it rapidly decreases with depth. This means that the annual averaging is permissible without applying a seasonal correction only below 200-300 m, but not above.

Given the critical roles played by temperature and salinity changes in all other oceanographic variables and processes, the metrics of the seasonal cycle presented and discussed in this report have significant implications to all other disciplines and rationalization of various field activities.
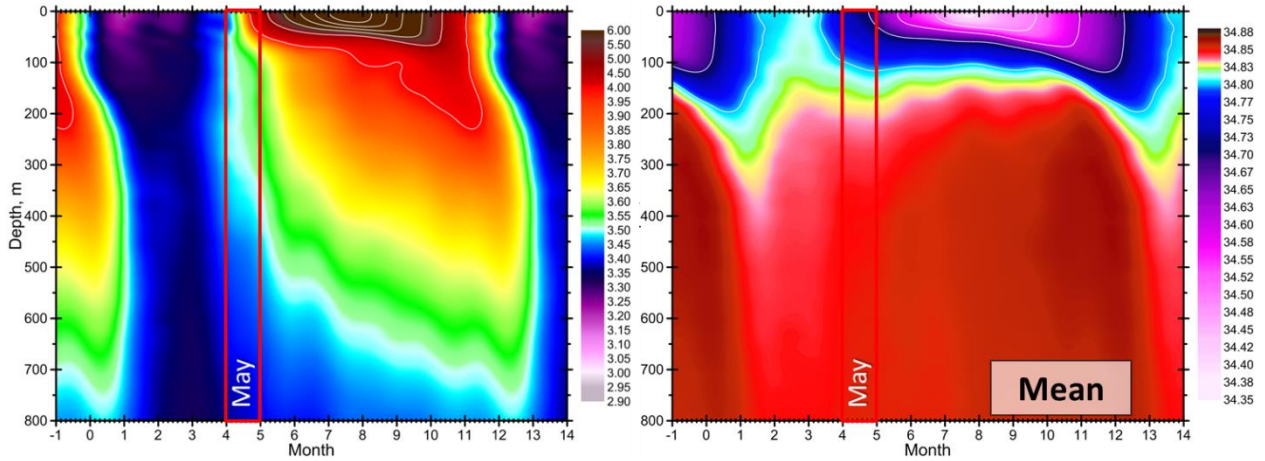
Figure A1. Regular seasonal cycles of temperature (left) and salinity (right) in the central Labrador Sea based on the iterative time series analysis technique by Yashayaev applied to all ship and Argo data.
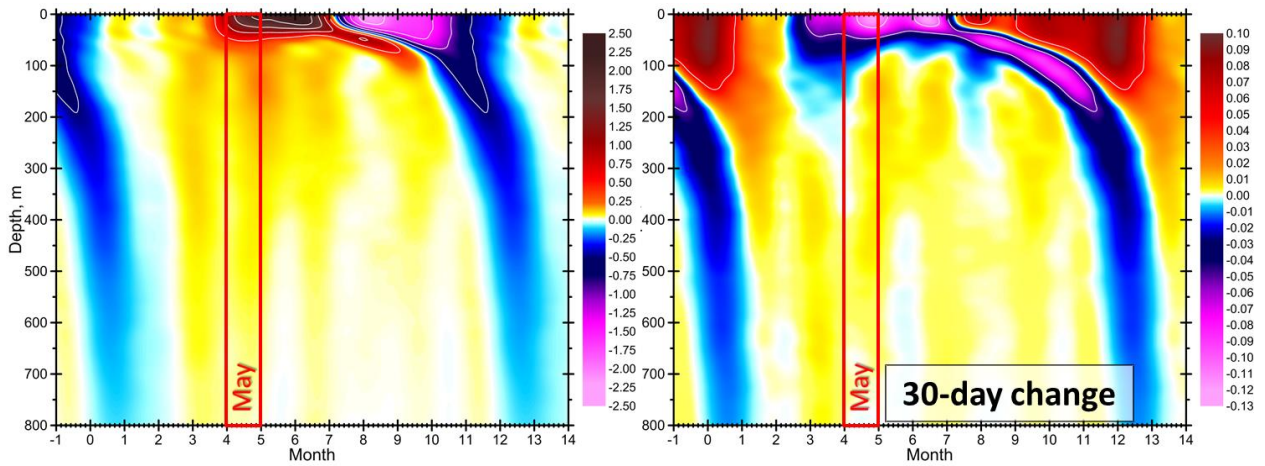

Figure A2. Ranges of temperature (left) and salinity (right) climatological normal values, shown in Figure A1, confined to 30-yearday-long seasonal intervals starting at each consecutive yearday.
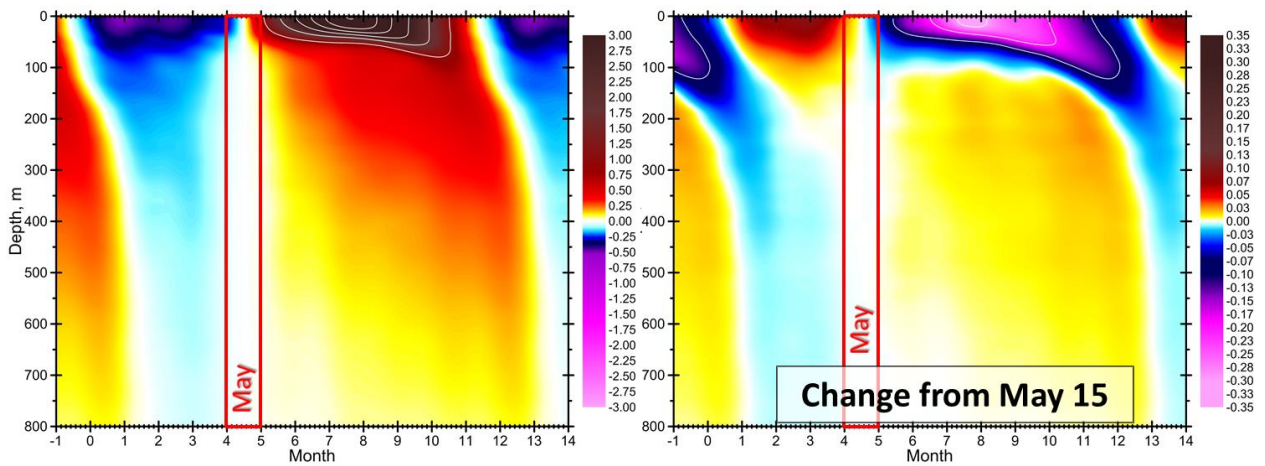
Figure A3.   Seasonal changes of temperature (left) and salinity (right) referenced to the 15th of May (zero changes on that day).
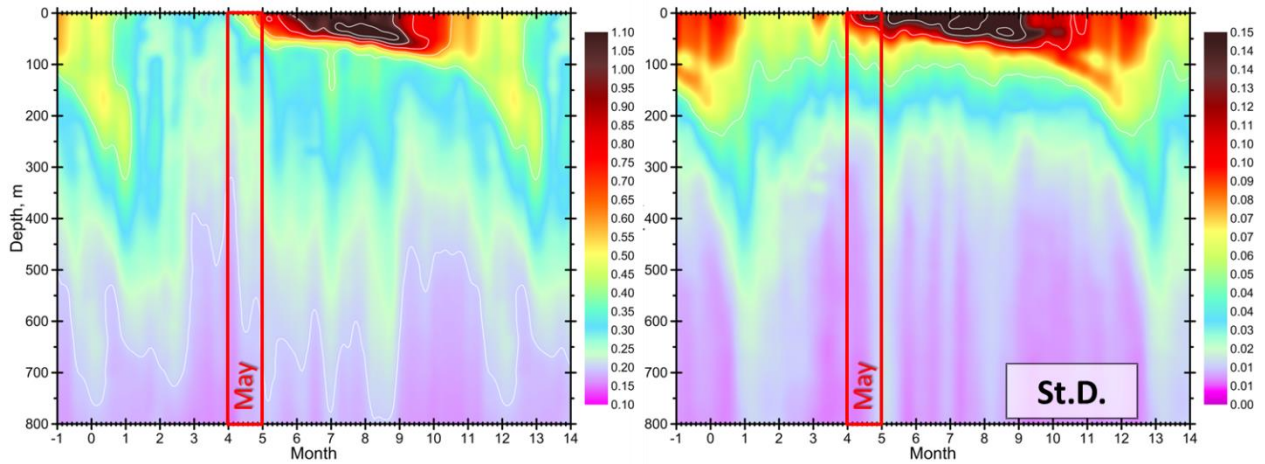

Figure A4.   Standard deviations of temperature (left) and salinity (right) anomalies in the central Labrador Sea computed for data from all years selected within individual 10-yearday-long seasonal bins. The starting points of these bins are separated by 5 yeardays. The anomalies were computed by subtracting the harmonic seasonal cycle (Figure A1) from all multiyear observations at each depth. The data have been quality controlled (outliers removed) using the iterative seasonal cycle estimation techniques. Note that the standard deviations of temperature anomalies is smaller than the 30-day seasonal temperature change in May (Figure A2)
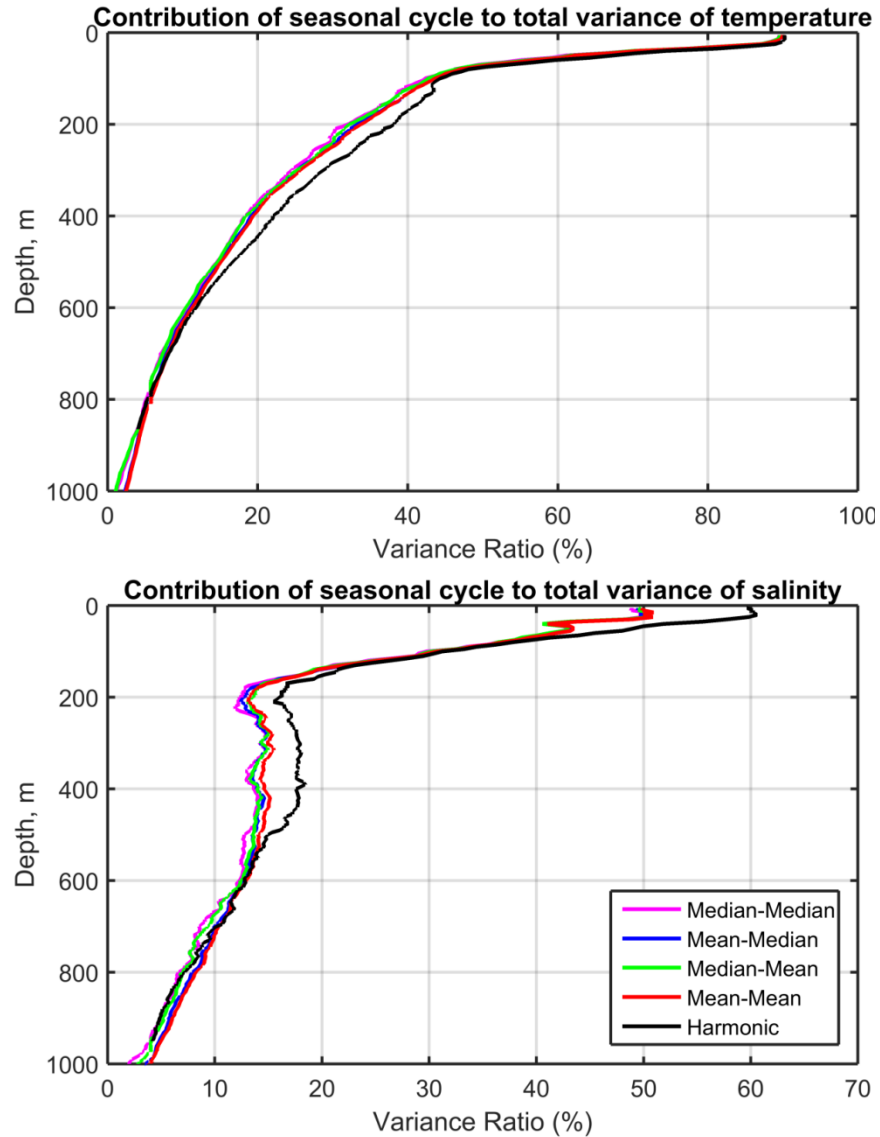
Figure A5. Contribution of computed seasonal cycle to the total variance of temperature (top) and salinity (bottom). The seasonal cycles were estimated by using data binning with 10-day bins spaced at 5-day intervals (*coloured lines*) and by using the iterative time series analysis technique based on harmonic analysis (*black line*) developed by Yashayaev. The data have been quality-controlled (outliers removed) as part of the same time series analysis.
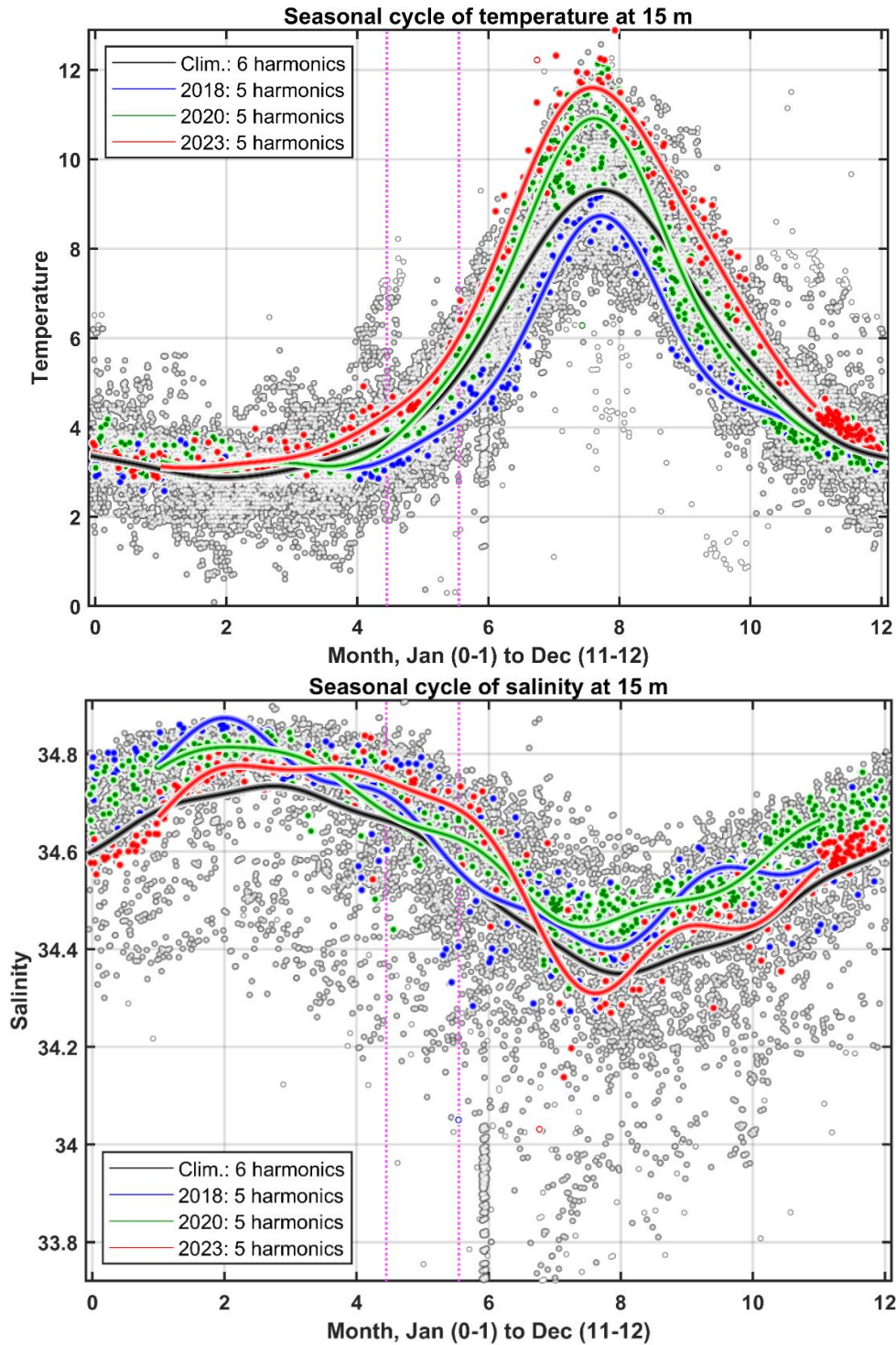
Figure A6. Temperature (*upper panel*) and salinity (*lower panel*) measurements at 15 m depth level in the central Labrador Sea (Figure 1) for the period of 1948-2023 with respect to decimal month. The 2018, 2020, and 2023 data values, and associated seasonal cycles are shown with *blue*, *green*, and *red dot clouds*, and *lines*, respectively. The *black line* represents the all-data climatological (regular or normal) seasonal cycle. The *vertical magenta dotted lines* confine the time period from May 15 to June 15.